P
2 mix

Fore-and-Aft Elastic Response Characteristics of Size 34x9.9, Type VII, 14 Ply-Rated Aircraft Tires of Bias Ply, Bias-Belted, and Radial-Belted Design

By

John Albert Tanner

B.S. July, 1966, North Carolina State University

A Thesis submitted to

The Faculty of

The School of Engineering and Applied Science

of The George Washington University in partial satisfaction

of the requirements for the degree of Master of Science

May 6, 1973

NASA-TM-X-69570) FORE AND AFT ELASTIC RESPONSE CHARACTERISTICS OF SIZE 34X9.9, TYPE 7, 14 PLY-RATED AIRCRAFT TIRES OF BIAS PLY, BIAS BELTED, AND RADIAL BELTED DESIGN (NASA) 66 ~~65~~ p HC $5.25 CSCL 01C

N73-28987

Unclas

G3/02 12178

ABSTRACT

An investigation was conducted to determine the fore-and-aft elastic response characteristics of size 34 x 9.9 type VII aircraft tires of bias ply, bias-belted, and radial-belted design. The investigation consisted of static and rolling tests at the Langley Aircraft Landing Loads and Traction Facility; a statistical analysis which related the measured tire elastic characteristics to variations in the vertical load, inflation pressure, braking force and/or tire vertical deflection, and a semi-empirical analysis which related the tire elastic behavior to measured wheel slippage during steady-state braking.

The results of this investigation indicate that the bias-belted tire has the largest spring constant value for most loading conditions and the radial-belted tire has the smallest spring constant value. The elastic response of the tire free-tread periphery to static braking was shown to include both tread stretch and carcass torsional wind-up about the axle for the bias ply and bias-belted tires and carcass wind-up alone for the radial-belted tire. Tread stretching under braked rolling conditions was detected within the footprints of the bias ply and bias-belted tires but not within the footprint of the radial-belted tire. It was demonstrated that changes in the rolling radius due to braking can be predicted with reasonable accuracy from the tire fore-and-aft elastic response characteristics. Finally, the tire slippage during steady-state braking was shown to be greater for the bias ply tire than for the bias-belted and radial-belted tires.

TABLE OF CONTENTS

LIST OF TABLES

LIST OF FIGURES

INTRODUCTION

The most costly maintenance item associated with aircraft landing gear systems is the replacement of worn or damaged aircraft tires (reference 1). One of the more promising approaches to increased tread life, which has proven successful in automative applications, is to replace conventional bias ply tires with either bias-belted or radial-belted tires. This approach could also result in an improvement in the cornering and braking traction available to the aircraft if the belted carcass design reduces tire scrubbing and associated heat generation within the footprint during ground maneuver operations as advertised by tire manufacturers. However, since the bias-belted and radial-belted designs differ from that of the conventional bias ply tire then it is reasonable to speculate that the elastic response characteristics of these tires will also differ.

In 1965 reference 2 presented the results of an analog computer model study which indicated that the braking performance of aircraft antiskid braking systems, which produced a cyclic braking effort , could be affected by the elastic response characteristics of aircraft tires in the fore-and-aft or braking direction. The results of this computer study were later corroborated by experimental data (reference 3). In their operation those antiskid systems control the application of brake torque by sensing wheel angular velocity and/or acceleration. However, because of the elastic behavior of the tire the angular velocity and acceleration of the wheel can differ significantly from that of the tire particularly at the tire-pavement interface where the braking traction is actually developed. This spring coupling between the brake and the pavement influences the operational behavior of the antiskid braking systems. Therefore a knowledge of the fore-and-aft elastic response characteristics of aircraft tires is necessary for safer and more economical operations of aircraft antiskid braking systems.

References 4 to 11 are examples of early (1940 - 1958) research papers which studied tire elastic response characteristics. These early studies dealt primarily with tire lateral deformations since wheel shimmy was a serious problem in the automotive and aircraft industries, and sophisticated aircraft antiskid systems were still years away from development. In 1965 when reference 2 was published, the information on tire fore-and-aft elastic response characteristics was limited to a few static data points (reference 12) and an empirical analysis (reference 13) based entirely upon the free-tread peripheral measurements presented in reference 12. Reference 14, published in 1971, studied the fore-and-aft elastic response characteristics of bias ply aircraft tires in more detail, but no data exists which describes the fore-and-aft elastic response characteristics of bias-belted and radial-belted aircraft tires.

The purpose of this paper is to present the results of an investigation to determine the fore-and-aft elastic response characteristics of size 34 x 9.9, type VII, 14 ply rated aircraft tires of bias ply, bias-belted, and radial-belted construction. These characteristics which include fore-and-aft spring constant, fore-and-aft decay length along the free-tread periphery, and displacement variation within the rolling footprint were obtained over a range of vertical loads from 51.2 kN (11500 lbs) to 66.8 kN (15,000 lbs) and inflation pressures from 62 N/cm^2 (90 lbs/in^2) to 97 N/cm^2 (140 lbs/in^2) at ground speeds up to 100 knots and at braking forces up to 22.3 kN (5000 lbs). The investigation consisted of static and rolling tests at the Langley Aircraft Landing Loads and Traction Facility; a statistical analysis which related the measured tire elastic characteristics to variations in the vertical load, inflation pressure, braking force, and/or tire vertical deflection; and a semi-empirical analysis which related tire elastic behavior to measured wheel slippage during steady-state braking.

SYMBOLS

Measurements and calculations were made in U. S. Customary Units and converted to S.I. units. Values are given in both S.I. and U.S. Customary Units.

a,b	displacements
D	distance
e	base of natural logarithms
F_x	braking force
F_z	vertical load
h	footprint half length
J	decay length
K_x	static fore-and-aft spring constant
M	rolling footprint deformation variation
m	linear slope
N	number of wheel revolutions
P	inflation pressure
Q	tread stretch
R	rolling radius
r, r^2	statistical correlation coefficients
S	tire circumferential distance
u	deformation, displacement
X_T	total tire slippage
$\alpha, \beta, \gamma, \eta$	generalized constants
δ	tire vertical deflection

ΔR	change in rolling radius
ε_x	elongation strain due to braking
μ	coefficient of friction

Subscripts

b	braked
calc	calculated
exp	experimental
f	footprint
f_0	center of footprint
max	maximum value
0	unbraked
p	free tread periphery
p_i	peripheral station
p_0	footprint leading edge
T	total
X	fore-and-aft
Z	vertical

APPARATUS AND TEST PROCEDURE

Test Tires

The tires of this investigation were size 34 x 9.9, type VII, 14 ply rated aircraft tires of bias ply, bias-belted, and radial-belted design. Figure 1 is a photograph of the tires before testing and the shape of the tire footprint under rolling conditions is shown in figure 2. The differences in tire construction are illustrated by the sketches in figure 3. The bias ply tire is constructed with the carcass plies arranged on a bias to form a relative angle between the reinforcing chords of alternating plies. The carcass is then capped with the tire tread. The bias-belted tire is constructed in the same manner as the bias ply tire except that a circumferential reinforcing belt is added to the carcass. The radial-belted tire is constructed with the reinforcing chords of the carcass plies oriented radially about the tire. The carcass is then reinforced with a circumferential belt and capped with the tire tread. Specifications for the three tires are presented in table I.

Test Facility

In its present configuration, the Langley Aircraft Landing Loads and Traction Facility (formerly called the Landing Loads Track) consists of a rail system 671 m (2200 ft.) long by 9.1 m (30 ft.) wide, a large hydraulically operated water-jet catapult system, an arresting system, and two test carriages. A schematic of the facility is presented in figure 4 and a aerial photograph is shown in figure 5. The

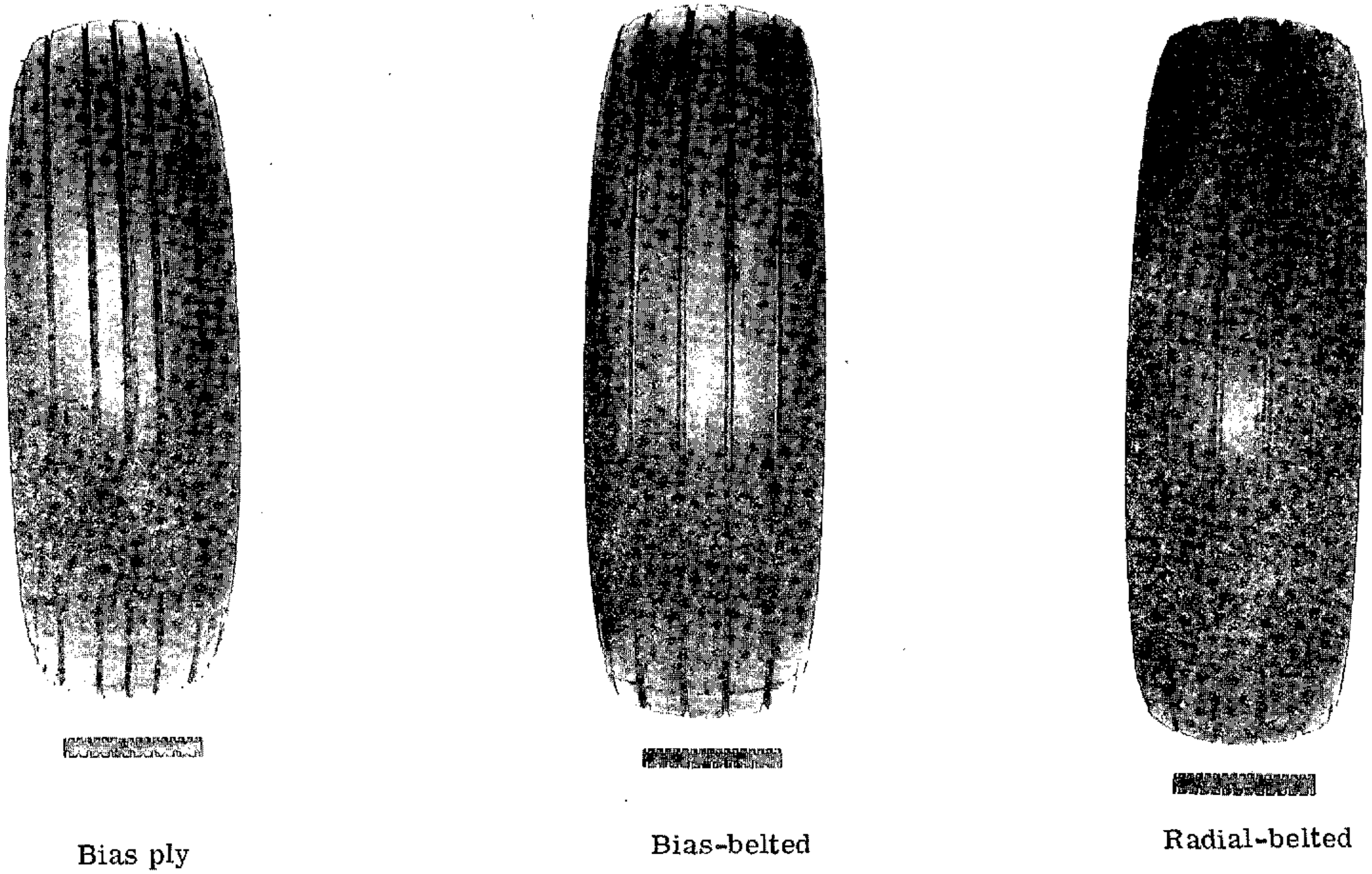

Figure 1.- Aircraft tires used in the investigation.

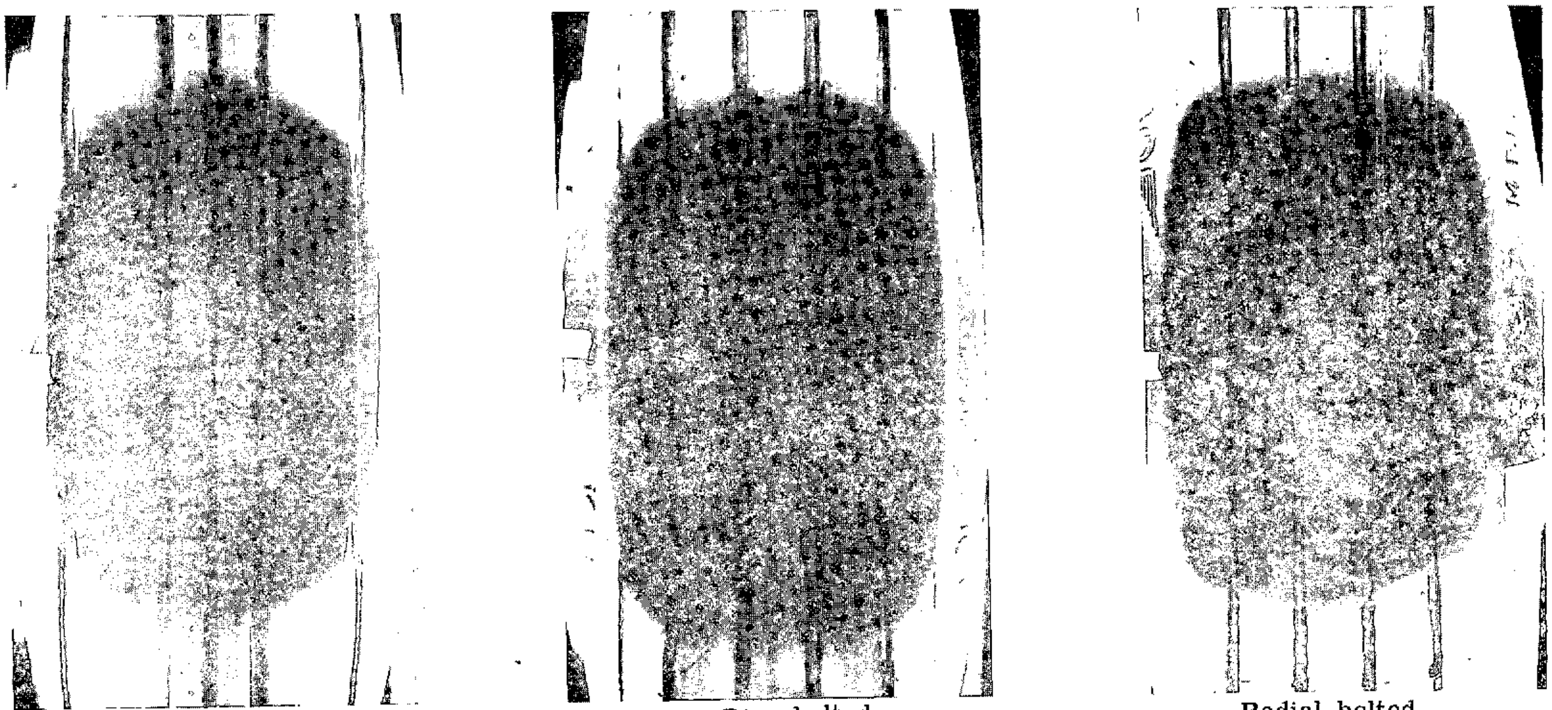

Bias ply Bias-belted Radial-belted

Figure 2.- Tire footprints as seen from beneath glass plate.

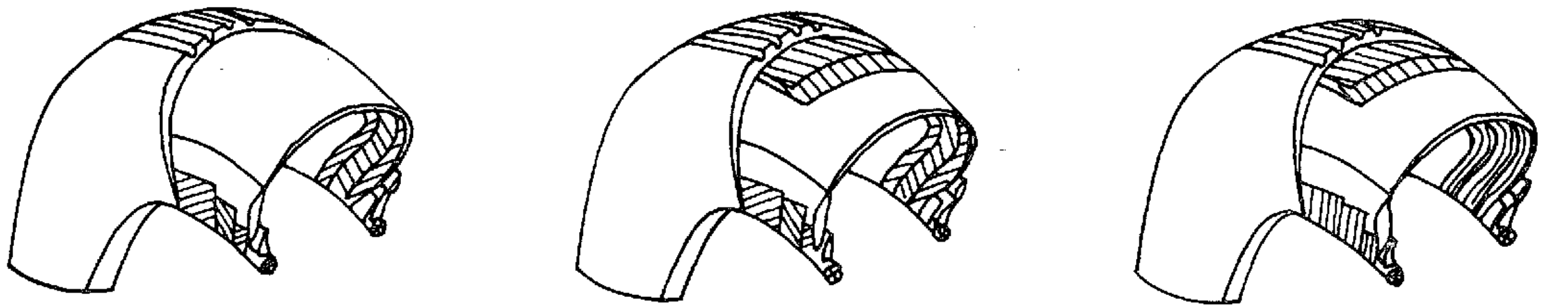

Bias ply   Bias-belted   Radial-belted

Figure 3.- Sketches illustrating the different tire constructions.

TABLE I.- TIRE SPECIFICATIONS

Item	Bias Ply	Bias-belted	Radial-belted
Bead	Wire, steel	Wire, steel	Wire, steel
Carcass Matrix Chord	 Natural rubber Nylon	 Natural rubber Nylon	 Natural rubber Nylon
Belt	None	Polyester	Steel
Tread Material Groove pattern	 Natural rubber 5-Groove	 Natural rubber 4-Groove	 Natural rubber 4-Groove
Rated inflation pressure	79 N/cm^2 115 lb/in^2	79 N/cm^2 115 lb/in^2	79 N/cm^2 115 lb/in^2
Rated vertical load	58.7 kN 13,200 lbs	58.7 kN 13,200 lbs	58.7 kN 13,200 lbs

central feature of the catapult system is an L-shaped pressure vessel containing 37.9 m^3 (10,000 gallons) of water. This vessel is pressurized with air, up to 2207 N/cm^2 (3200 lb/in^2), and a timed, quick-acting valve at the front of the vessel releases a high energy jet of water through a 17.78 cm (7 inch) diameter nozzle which impinges upon an U-shaped turning bucket at the rear of the test carriage. The catapult can develop approximately 2002.5 kN(450,000 lbs) of thrust which is sufficient to accelerate either test carriage to speeds of 120 knots in 2.5 - 3 seconds over about 122 m (400 ft.). After accelerating to the desired speed, the test carriage coasts through the test section of the facility, about 368 m (1200 ft.), and is brought to a stop by 5 parallel arresting cables which are interconnected to 20 Navy Mark IV arresting gear engines.

Both the static and rolling tests were conducted with the wheel, tire, and brake assembly mounted in an instrumented yoke dynamometer which was attached to the center drop frame of the large test carriage. This carriage, shown in figure 6, weighs approximately 534 kN (120,000 lbs). The dead weight of the drop frame was 51.2 kN (11500 lbs) and was down-loaded hydraulically to increase the tire vertical loading. For the tests described in this paper the test runway had a concrete surface with a light broom finish. This surface was somewhat smoother than those of most operational runways. A camera pit was installed in the test runway at its mid-length and covered with a glass plate 228.6 cm (90 in) long by 121.9 cm (48 in) wide by 20.3 cm (8 in) thick which was mounted flush with the concrete surface. This glass plate can

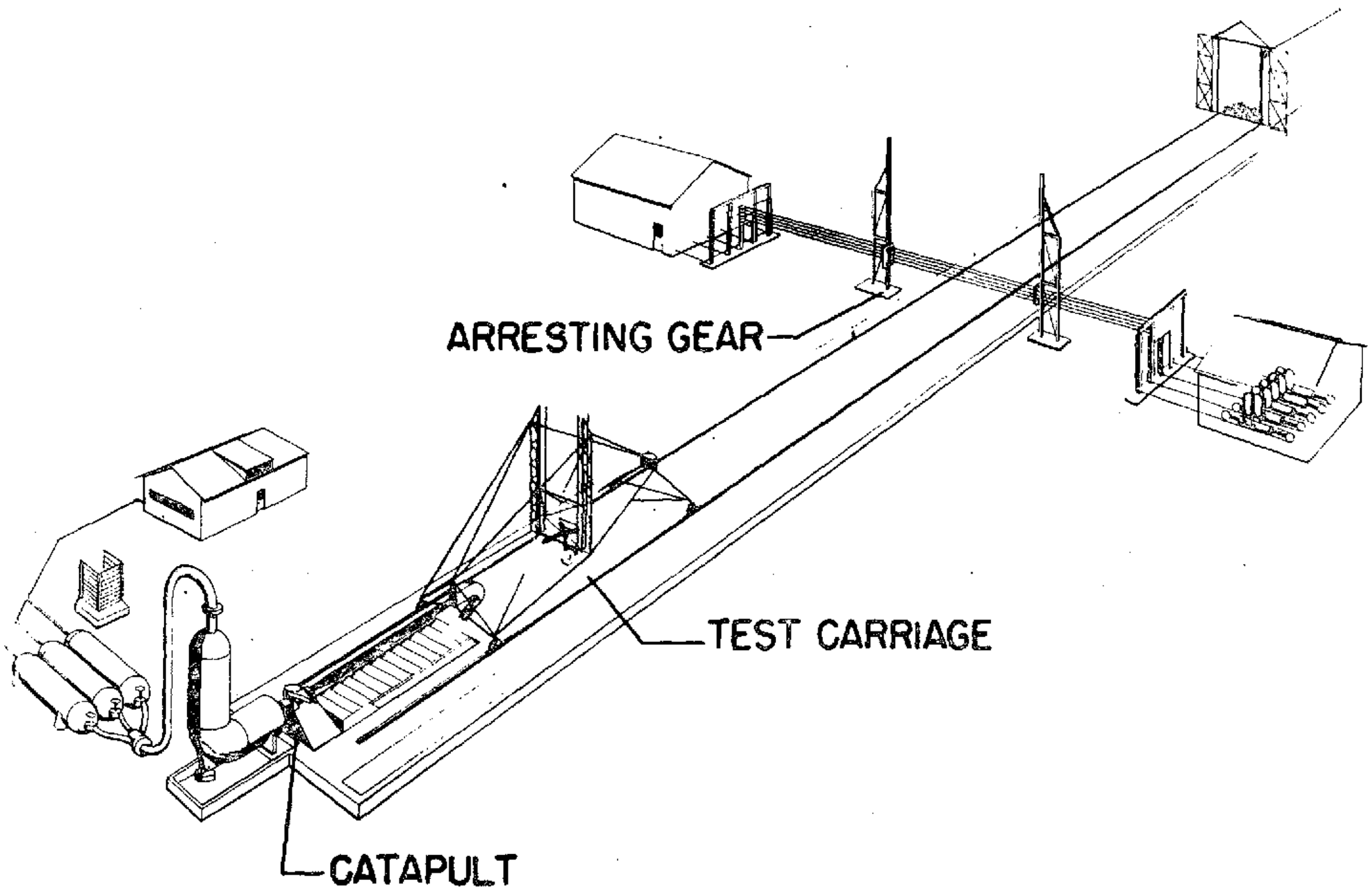

Figure 4.- Schematic of aircraft landing loads and traction facility.

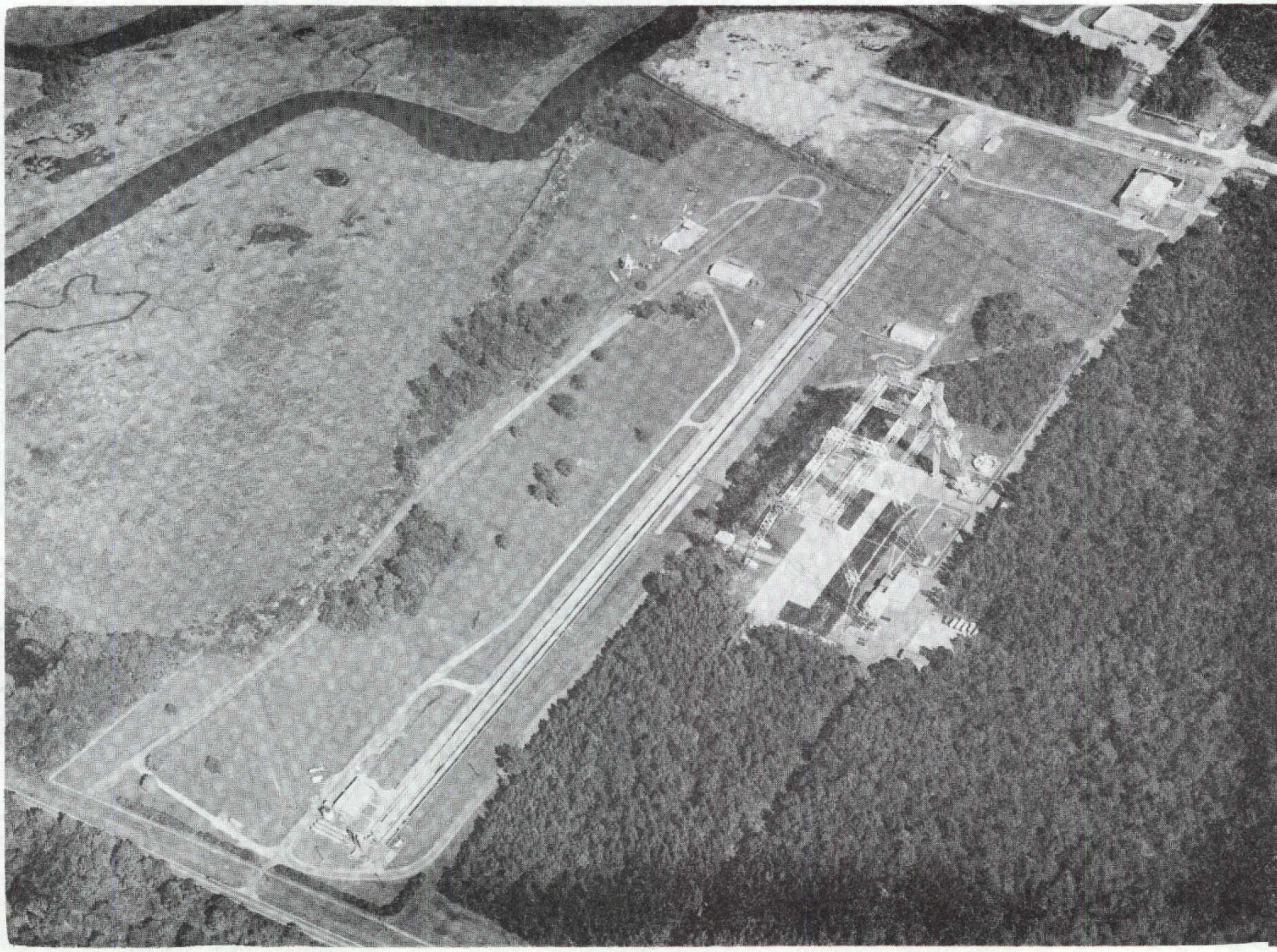

Figure 5.- Aerial photograph of test facility.

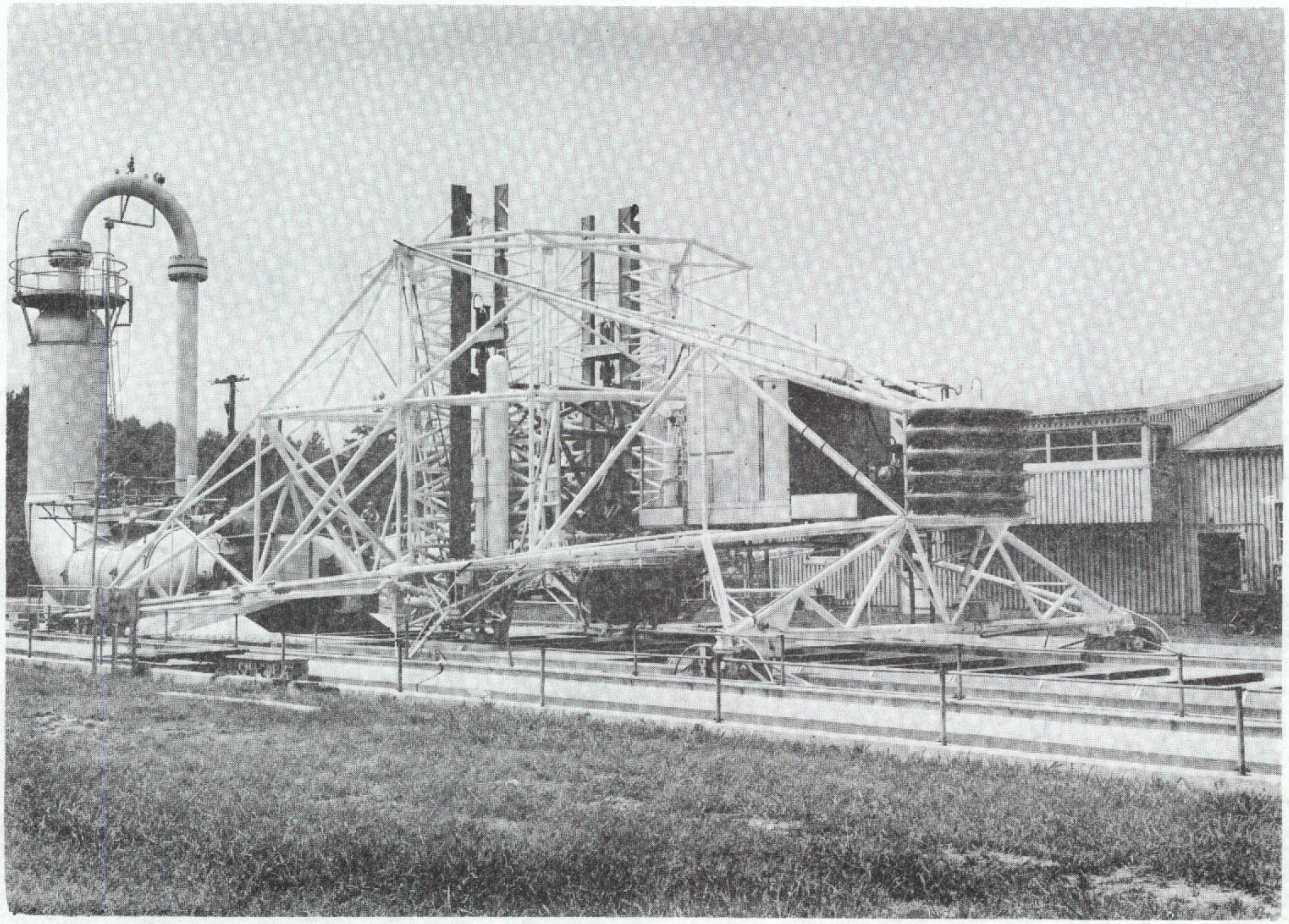

Figure 6.- Test carriage and L-shaped pressure vessel.

withstand a 178 kN (40,000 lb) load at its mid-span. The glass plate was cleaned and dried before each test and the friction forces developed on its surface were comparable to those developed on the concrete surface.

Static Tests

The objectives of the static tests were to determine the tire fore-and-aft spring constants and to measure the deformation or stretch along the free-tread periphery. Two different test procedures were required to meet these objectives and each is described separately in the paragraphs which follow.

Spring constants.- Figure 7 is a photograph of the test equipment employed to determine the fore-and-aft spring constants of the test tires. This equipment consisted of the test tire which rested, under a vertical load, on the surface of a bearing plate and the instrumentation necessary to monitor the tire loadings and the bearing plate displacements. The carriage and wheel were externally braced to prevent axle translation and wheel rotation. Tire loadings included the vertical load which was controlled by the carriage hydraulic system and the fore-and-aft, or static braking force, which was applied to the bearing plate by means of a hydraulic piston. The magnitude of the vertical load applied to the tire was measured by load cells under the bearing plate, and the braking force was measured by a load cell located between the hydraulic piston and the backstop. The braking forces were restricted to levels insufficient to produce any discernible slippage in the tire—bearing-plate interface. Fore-and-aft displacements of the bearing plate during brake force applications were obtained from a dial gauge graduated into thousandths of an inch. Since there was no relative motion (no slippage) between the tire footprint and the bearing plate, those bearing-plate displacements corresponded to the footprint displacements with respect to the axle. The testing technique involved the application of the desired vertical load to the tire , the incremental application of braking force, and the recording of the resulting displacements of the footprint with respect to the axle.

Deformation in the free-tread periphery.- Deformations in the free-tread periphery were measured concurrently with the spring constants. In preparation for these measurements, a number of cone-shaped rubber studs were attached along the periphery of each tire as shown in figure 7 and a camera was mounted to a beam which was free to rotate about the axle center line. Free-tread periphery deformations were obtained from projected enlargements of photographs taken of the studs during the course of the static tests.

Rolling Tests

The objectives of the braked-and unbraked-rolling tests were to measure the deformation or stretch within the footprint and to determine the braked and unbraked apparent tire rolling radii. Two different test procedures were required to meet these objectives and each is described separately.

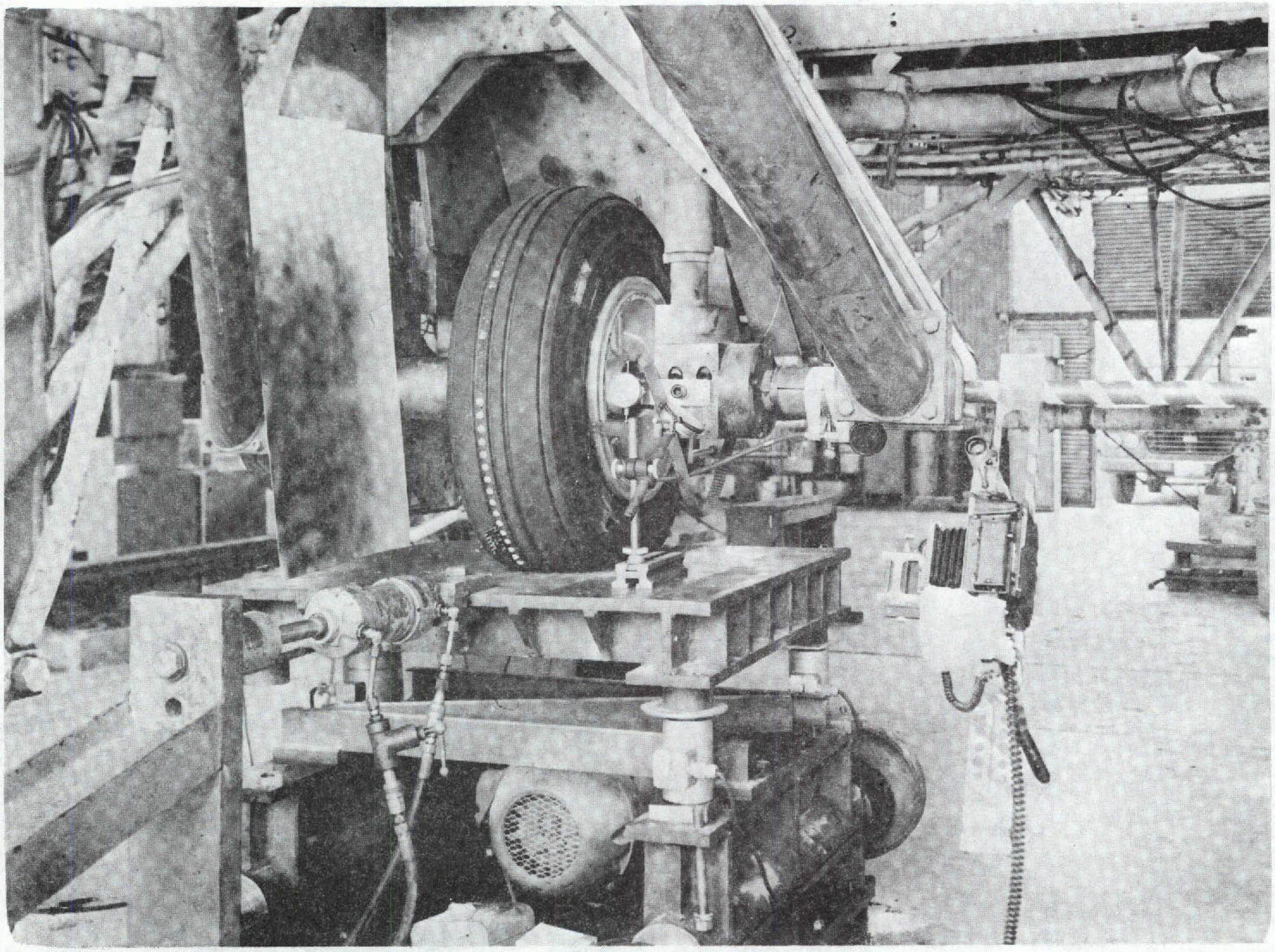

Figure 7.- Static test equipment.

Deformation within the footprint.- Figure 8 is a photograph of the carriage during tests to determine the deformation within the rolling footprint. The deformations resulting from the combined vertical and braking forces on the tire were determined from projected enlargements of photographs of the tire footprint taken through the glass plate installed in the runway. In preparation for these tests, equally spaced small holes 3.2 mm (1/8 in) in diameter and 1.6 mm (1/16 in) deep were drilled along the tread periphery, and filled with a white silicon rubber as shown in figure 2. The test procedure envolved rolling the tire, under the desired vertical load, over the glass plate at a speed of approximately 5 knots. The brake pressure was preset at values which were sufficient to develop the desired braking force but incapable of producing a locked-wheel skid and photographs were taken of the passing footprint.

Braked and unbraked tire rolling radii.- These tests were conducted on the dry concrete runway at the desired vertical loads, inflation pressures, and braking forces. The test procedure envolved towing or catapulting the carriage to the desired speed, applying the desired loads, and recording the load and displacement data as time histories on a recording oscillograph. Measurements of the vertical load and braking force were obtained from the instrumented dynamometer and the braked and unbraked apparent tire rolling radii were determined from measurements of the distance traveled along the runway and the angular displacement of the wheel.

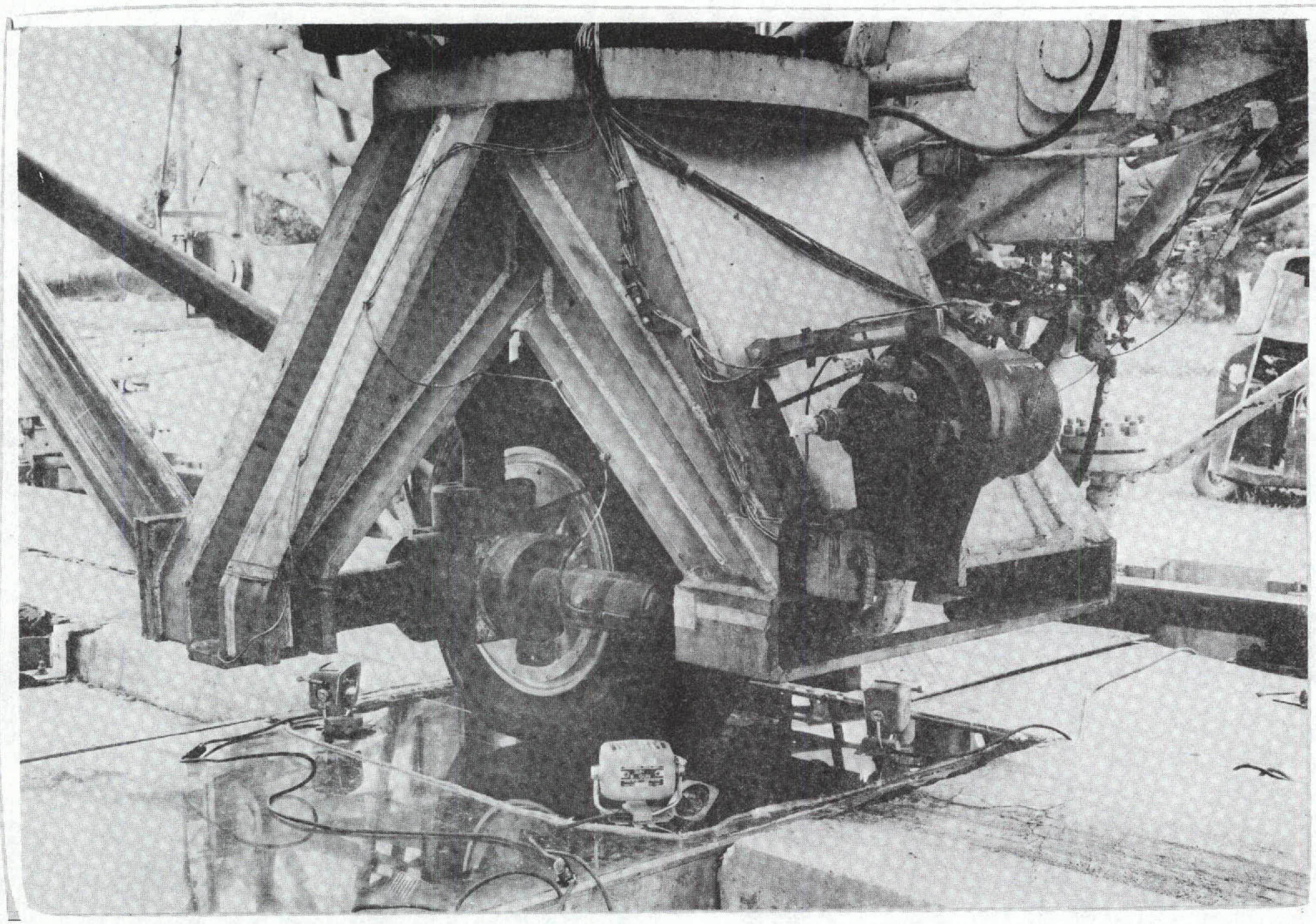

Figure 8.- Tire and instrumented dynamometer during braked-rolling test over glass plate.

Statistical Analysis

Statistical analysis techniques were used to establish linear relationships between the tire fore-and-aft elastic response characteristics and the loading parameters. Three different techniques were used in this investigation and each is briefly noted.

Method of least squares.- When a relationship between two variables was needed, the method of least squares (reference 15) was used to determine the best unbiased estimate of the linear relationship and to define the correlation coefficient.

Multiple regression analysis.- When a relationship between tire fore-and-aft elastic response characteristics and several loading parameters was needed, a multiple regression analysis (reference 16) was performed to determine the matrix of coefficients and to define the degree of correlation.

Analysis of variance rationale.- When it was necessary to determine which loading parameters had a significant effect on the tire fore-and-aft elastic response characteristics, the analysis of variance rationale (reference 17) was used to construct an ANOVA table and a test for significance based on the F distribution table (reference 17) was performed.

RESULTS AND DISCUSSION

Force and displacement measurements on bias ply, bias-belted, and radial-belted aircraft tires were obtained under both static and rolling conditions. The static measurements were used to define the tire fore-and-aft spring constant and to establish the tread stretch distribution along the free-tread periphery near the footprint leading edge due to the braking effort. The rolling measurements were used to establish the tread stretch distribution within the leading portion of the footprint and the apparent change in rolling radius due to the braking effort. The following sections discuss the variation of these tire elastic characteristics with vertical load, tire vertical deflection, inflation pressure, and braking force and include a discussion of variations in the tire rolling radius and their effect on both wheel and tire slippages.

Static Response

Fore-and-aft spring constant.- The fore-and-aft spring constant K_x is a fundamental property which defines the elastic deformation of the tire when subjected to a braking force. This spring constant takes into account both the circumferential deformation of the tread and the torsional wind up of the carcass resulting from brake application and is therefore, a measure of the overall elastic response of the braked tire. This property was obtained experimentally for each tire under various vertical loads and inflation pressures by relating the braking force to the footprint displacement with respect to the axle.

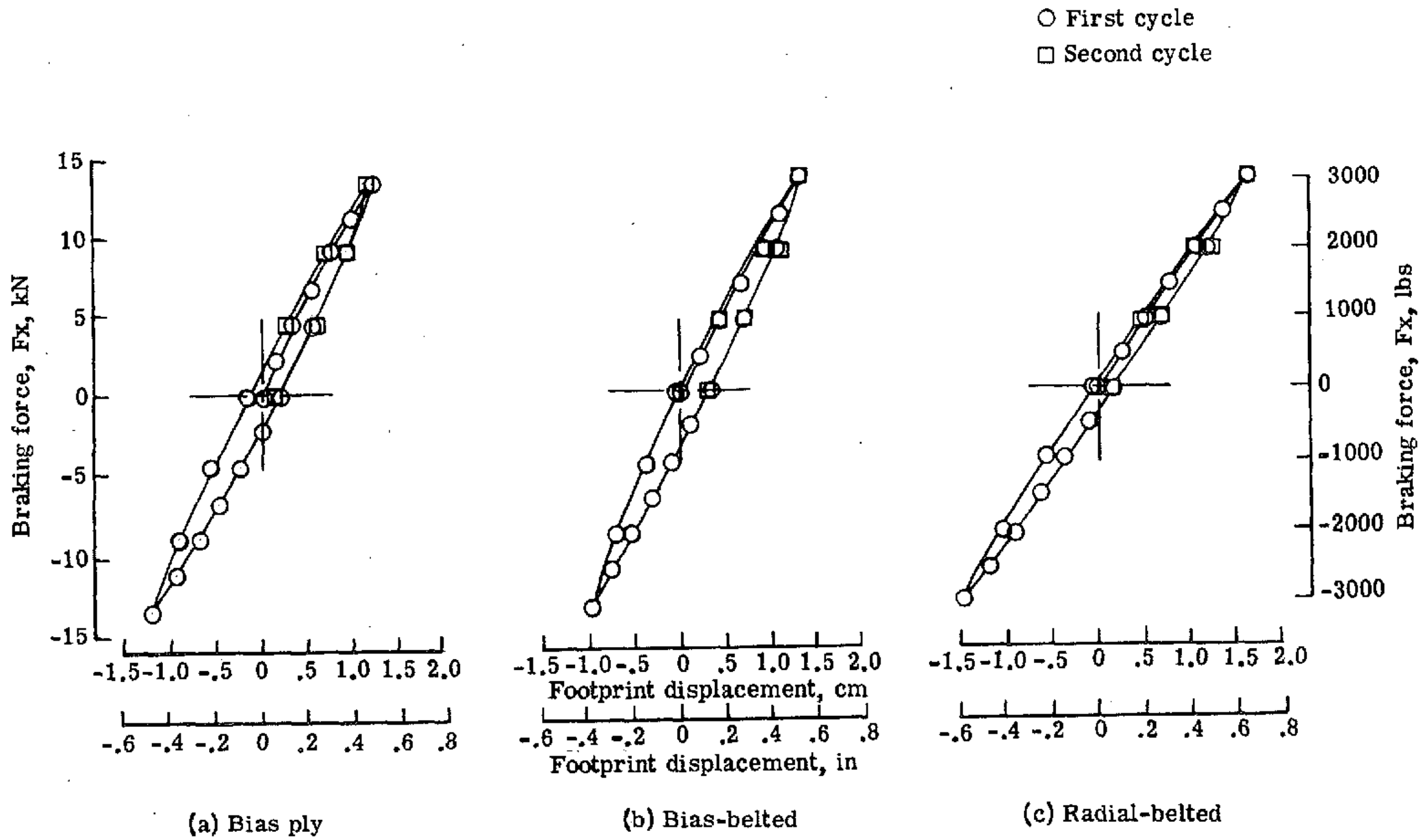

Figure 9.- Typical fore-and-aft load-deflection curves. F_z = 58.7 kN (13200 lbs); P = 79 N/cm^2 (115 lb/in^2).

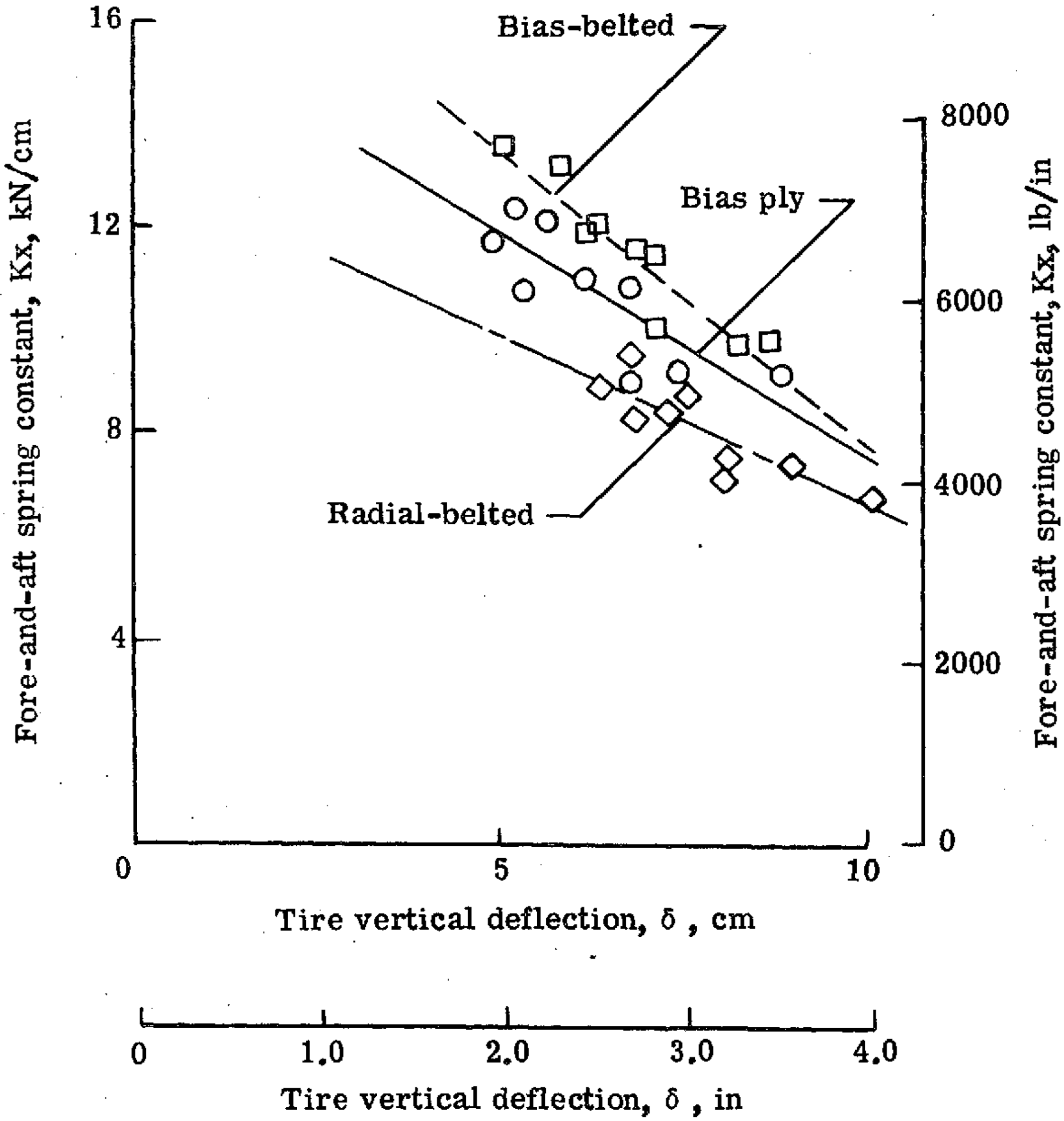

Figure 10.- Variation in fore-and -aft spring constant with tire vertical deflection.

TABLE II.- SUMMARY OF FORE- AND -AFT SPRING CONSTANTS FROM STATIC TESTS

Inflation pressure N/cm^2 lb/in^2	F_z, kN, lbs	Bias Ply		Bias-belted		Radial-belted	
		k_x, kN/cm lb/in	δ, cm in.	k_x, kN/cm lb/in	δ cm in.	k_x kN/cm lb/in	δ, cm in.
62 90	51.2 (11,500)	9.00 5133	6.83 2.69	10.01 5709	7.14 2.81	7.47 4260	8.10 3.19
	58.7 (13,200)	9.19 5240	7.47 2.94	9.69 5525	8.26 3.25	7.44 4240	9.04 3.56
	66.8 (15,000)	9.17 5226	8.89 3.50	9.88 5634	8.74 3.44	6.80 3879	10.16 4.00
79 115	51.2 (11,500)	10.83 6173	5.56 2.19	11.84 6749	6.20 2.44	8.26 4710	6.83 2.69
	58.7 (13,200)	11.04 6296	6.20 2.44	11.58 6601	6.83 2.69	8.63 4920	7.62 3.00
	66.8 (15,000)	10.86 6191	6.83 2.69	11.52 6565	7.14 2.81	7.96 4045	8.10 3.19
97 140	51.2 (11,500)	11.74 6696	4.93 1.94	13.61 7762	5.08 2.00	8.96 5110	6.35 2.50
	58.7 (13,200)	12.37 7051	5.38 2.12	13.19 7519	5.87 2.31	9.54 5440	6.83 2.69
	66.8 (15,000)	12.15 6928	5.72 2.25	12.08 6889	6.35 2.50	8.45 4820	7.32 2.88

Typical fore-and-aft load-deflection data for bias ply, bias-belted, and radial-belted tires under static loading conditions are presented in figure 9. These data were obtained over one and one-half loading cycles to establish the complete hysteresis loops. The value of K_x was taken as the slope of the line which connected the end points of each loop. Spring constants and static vertical deflection data for each tire are presented in table II.

The variation of K_x with vertical deflection is shown in figure 10. The data presented in the figure indicate that K_x decreases with vertical deflection for all three tires and is in direct opposition to the trends reported in reference 13. The bias-belted tire is shown to have the highest values of K_x followed in order by the bias ply and radial-belted tires. The linear curves fairing the data were obtained by the least squares method and are represented by the following equations:

$$\left.\begin{aligned} K_x &= 16.25 \text{ kN/cm} - (.086 \text{ kN/cm}^2)\delta \\ K_x &= 9276 \text{ lb/in} - (125 \text{ lb/in}^2)\delta \\ &\text{with} \\ r &= -.82 \end{aligned}\right\} \text{bias ply} \qquad (1)$$

$$\left.\begin{aligned} K_x &= 19.26\ \text{kN/cm} - (.114\ \text{kN/cm}^2)\delta \\ K_x &= 10995\ \text{lb/in} - (165\ \text{lb/in}^2)\delta \\ &\text{with} \\ r &= -.93 \end{aligned}\right\}\ \text{bias-belted} \qquad (2)$$

$$\left.\begin{aligned} K_x &= 13.10\ \text{kN/cm} - (.064\ \text{kN/cm}^2)\delta \\ K_x &= 7476\ \text{lb/in} - (93\ \text{lb/in}^2)\delta \\ &\text{with} \\ r &= -.84 \end{aligned}\right\}\ \text{radial-belted} \qquad (3)$$

The magnitude of r is a measure of the correlation between the data and the faired curves and the sign of r is determined by the slope of the faired curves. The coefficients associated with the vertical deflection term in equations 1 through 3 indicate that the bias-belted tire also has the sharpest decrease in K_x with vertical deflection followed in order by the bias ply and radial-belted tires.

In an effort to obtain further insight into the variation of the data presented in table II, a multiple regression analysis was performed to investigate the influence of variations in the vertical load and inflation pressure on the value of K_x. The analysis assumed a linear relationship of the form

$$K_x = \alpha + \beta\, F_z + \gamma P \qquad (4)$$

and yielded the following set of equations.

$$\left.\begin{aligned} K_x &= 3.13 \text{ kN/cm} + (.0126 \text{ 1/cm})\, F_z + (.086 \text{ cm})P \\ K_x &= 1788 \text{ lb/in} + (.0320 \text{ 1/in})\, F_z + (33.84 \text{ in})P \\ &\text{with} \\ r^2 &\approx 1.00 \end{aligned}\right\} \text{Bias ply} \qquad (5)$$

$$\left.\begin{aligned} K_x &= 6.93 \text{ kN/cm} - (.0436 \text{ 1/cm})\, F_z + (.090 \text{ cm})P \\ K_x &= 3956 \text{ lb/in} - (.1108 \text{ 1/in})\, F_z + (35.35 \text{ in})P \\ &\text{with} \\ r^2 &\simeq 1.00 \end{aligned}\right\} \text{Bias-belted} \qquad (6)$$

$$\left.\begin{aligned} K_x &= 7.19 \text{ kN/cm} - (.0533 \text{ 1/cm})\, F_z + (.049 \text{ cm})P \\ K_x &= 4106 \text{ lb/in} - (.1354 \text{ 1/in})\, F_z + (19.94 \text{ in})P \\ &\text{with} \\ r^2 &\approx 1.00 \end{aligned}\right\} \text{radial-belted} \qquad (7)$$

The magnitude of r^2, which is a measure of the ability of the equations to fair the data, may be artificially high for equations

5 through 7 since only nine data points were used to develop each equation.

The equation for the bias ply tire (equation 5) indicates that K_x increases with the vertical load thereby corroborating the results presented in reference 14. However, the equations for the bias-belted and radial-belted tires (equations 6 and 7) indicate that K_x decreases with vertical load. All three equations indicate that K_x increases with the inflation pressure. This trend is contrary to the results presented in reference 13 wherein K_x was reported to the insensitive to variations in the inflation pressure for bias ply tires.

A comparison of the vertical load and inflation pressure coefficients for equation 5 sheds some interesting light on the bias ply data presented in figure 10. Since an increase in the vertical load produces an increase in the vertical deflection and an increase in the inflation pressure produces a decrease in the vertical deflection, equation 5 indicates that the variation in K_x with tire vertical deflection for the bias ply tire is primarily influenced by variations in the inflation pressure. Furthermore, since the magnitude of the spring constant gradients noted for each tire in equations 1 through 3 are ranked in the same order as the inflation pressure coefficients in equations 5 through 7, it appears that the bias-belted and radial-belted data presented in figure 10 are also primarily influenced by variations in the inflation pressure.

Free-tread periphery deformation distribution.- Experimental tests were performed to investigate the variation of tread deformation along the free periphery of each tire under static loading conditions. Figure 11 is a schematic representation of this deformation. As in references 13 and 14, it was assumed for these tests that the footprint deformed as a unit, i.e., no localized stretching within the static footprint. Further it was assumed that maximum tire deformation occurred at the leading edge of the footprint, therefore, during brake application the displacement of this point, identified as u_{p0} in figure 11(b), is defined by the ratio F_x/K_x. The displacements of other points along the free-tread periphery (μ_{pi} in the figure) were obtained by substracting from the maximum deformation the stretch accumulated between the leading edge of the footprint and the point in question.

A sample of the results from those tests are presented in figure 12 where the displacements are plotted on a logarithmic scale as a function of circumferential distance from the edge of the footprint on a linear scale. The deformations for the bias ply and bias-belted tires are shown initially to decay linearly from their maximum values as the circumferential distance from the footprint leading edge increases and then to remain essentially unchanged with a further increase in S_p. The deformation for the radial-belted tire are shown to remain constant regardless of the distance from the footprint leading edge.

The linearity of the data for all three tires in the region near the footprint leading edge indicate that there is an exponential relationship in that region between the tread deformation and the circumferential distance from the footprint leading edge. The equation

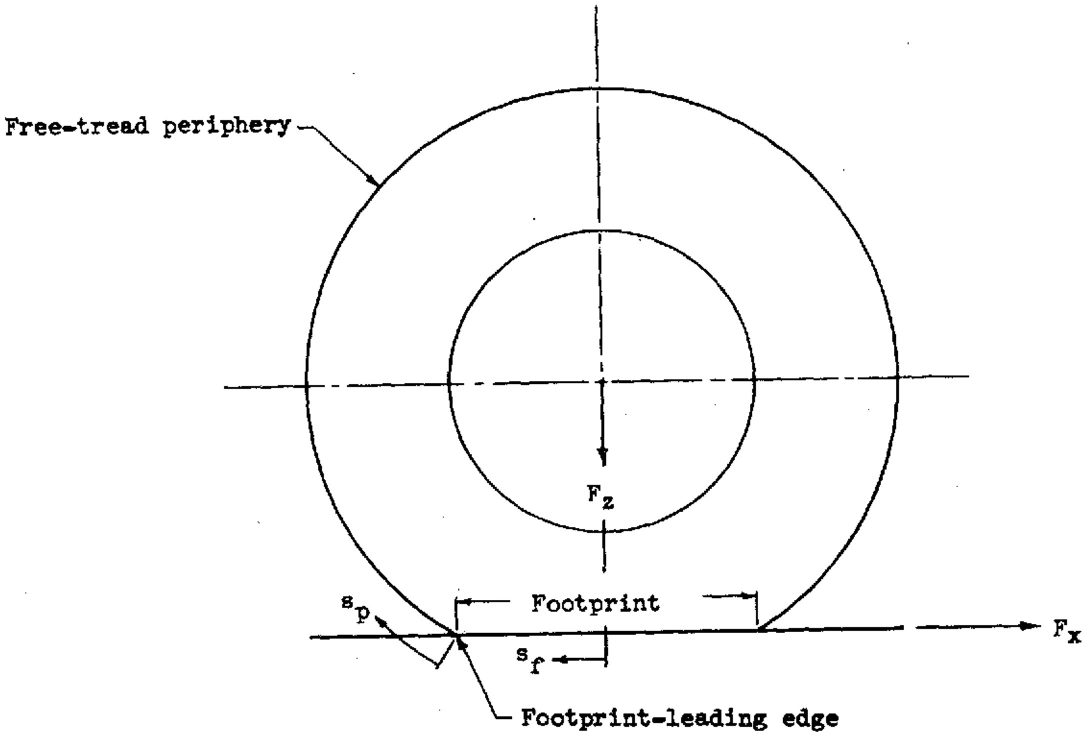

(a) Tire nomenclature.

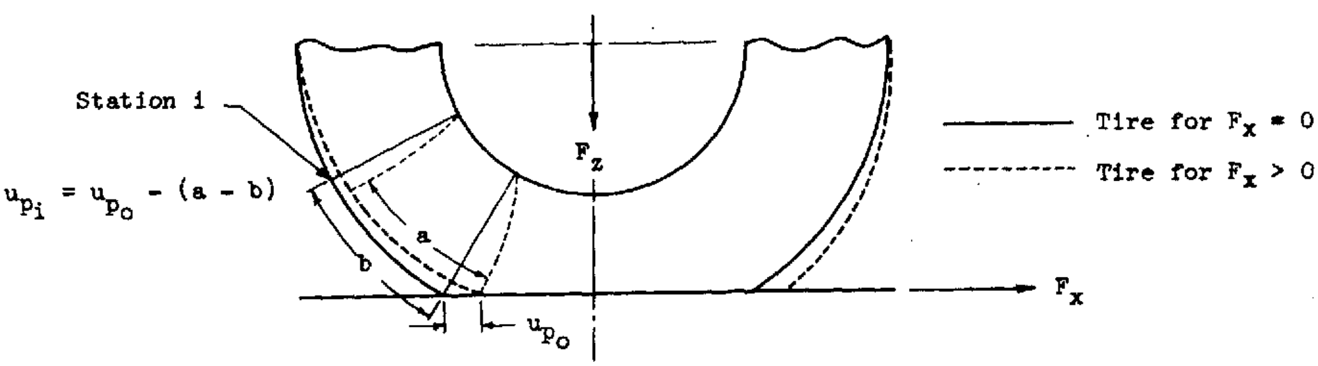

(b) Deformation in free-tread periphery.

Figure 11.- Sketches illustrating tire nomenclature and deformation in free-tread periphery under combined vertical load and braking force.

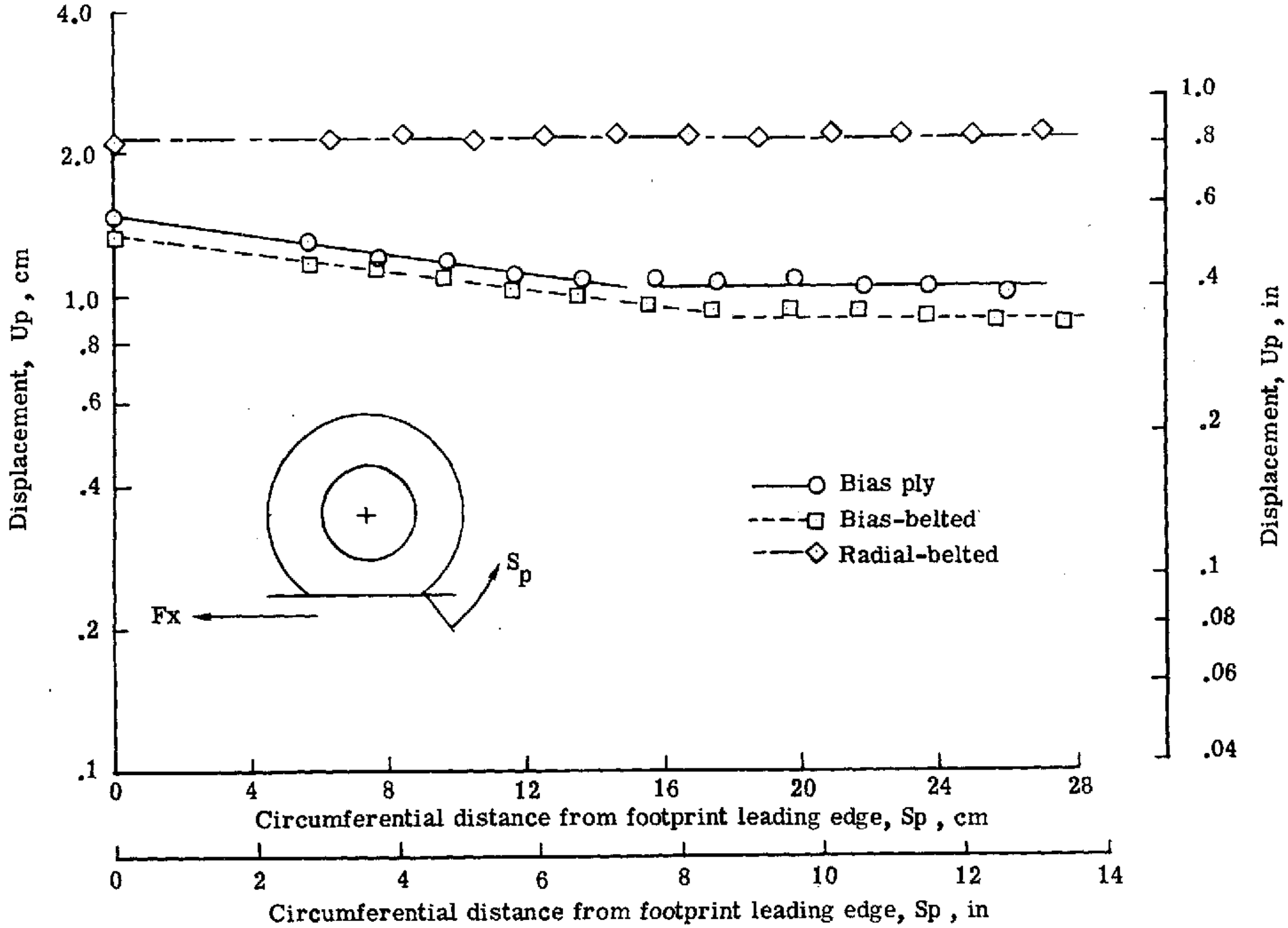

Figure 12.- Typical variation of displacements along free-tread periphery under static-loading conditions. Fz = 66.8 kN (15,000 lbs); P = 97 N/cm^2 (140 lb/in^2); Fx = 17.8 kN (4000 lbs).

which expresses this relationship is

$$u_p = \frac{F_x}{K_x} e^{-\frac{S_p}{J_x}} \qquad 0 \leq S_p \leq S_{p,max} \tag{8}$$

The slope of the equation is defined as $-\frac{1}{J_x}$ where J_x is referred to as the decay length and is a fundamental tire elastic property which defines the deformation distribution along the free-tread periphery. A small value of J_x indicates a tendency for the tread to stretch in the region near the footprint leading edge, and a large value of J_x indicates a tendency for the tread to deform as a unit with no stretching near the footprint during brake application. The data presented in figure 12 indicate that the elastic response of the bias ply and bias-belted tires to static braking forces includes both tread stretch in the immediate vicinity of the footprint and torsional deformation of the tire carcass about the axle. The elastic response of the radial-belted tire to static braking forces is shown to be strictly a torsional deformation of the carcass about the axle (no tread stretch).

A quantitative measure of the tire deformation along the free-tread periphery was obtained by setting the value of $S_{p,max}$ equal to 35.6 cm (14 in) and using the least squares method to compute J_x for each tire at various vertical loads, inflation pressures, and braking forces. These decay length values are presented in table

TABLE III.- SUMMARY OF FORE- AND -AFT DECAY LENGTHS FROM STATIC TESTS

(a) Bias ply tire; $S_{p,max}$ = 35.6 cm (14 in.)

Inflation pressure		F_z		F_x		J_x		r
N/cm^2	lb/in^2	kN	lbs	kN	lbs	cm	in.	
62	90	51.2	11500	8.9	2000	62.0	24.4	-.926
				13.4	3000	40.6	16.0	-.971
				17.8	4000	43.2	17.0	-.961
		58.7	13200	8.9	2000	186.9	73.6	-.633
				13.4	3000	51.6	20.3	-.944
				17.8	4000	58.7	23.1	-.953
		66.8	15000	8.9	2000	91.4	36.0	-.903
				13.4	3000	43.4	17.1	-.972
				17.8	4000	51.1	20.1	-.967
79	115	51.2	11500	8.9	2000	53.8	21.2	-.935
				13.4	3000	43.9	17.3	-.956
				17.8	4000	55.6	21.9	-.915
		58.7	13200	8.9	2000	83.8	33.0	-.876
				13.4	3000	46.2	18.2	-.959
				17.8	4000	51.8	20.4	-.944
		66.8	15000	8.9	2000	97.0	38.2	-.817
				13.4	3000	52.3	20.6	-.967
				17.8	4000	63.8	25.1	-.924
97	140	51.2	11500	8.9	2000	124.2	48.9	-.844
				13.4	3000	73.2	28.8	-.920
				17.8	4000	88.1	34.7	-.893
		58.7	13200	8.9	2000	88.1	34.7	-.804
				13.4	3000	72.9	28.7	-.905
				17.8	4000	65.0	25.6	-.915
		66.8		8.9	2000	117.6	46.3	-.852
				13.4	3000	67.1	26.4	-.967
				17.8	4000	89.4	35.2	-.929

TABLE III.- CONTINUED

(b) Bias-belted tire; $S_{p,max}$ = 35.6 cm (14 in.)

Inflation pressure		F_z		F_x		J_x		r
N/cm^2	lb/in^2	kN	lbs	kN	lbs	cm	in.	
62	90	51.2	11500	8.9	2000	†	†	†
				13.4	3000	59.2	23.3	-.962
				17.8	4000	66.0	26.0	-.949
		58.7	13200	8.9	2000	71.9	28.3	-.978
				13.4	3000	61.7	24.3	-.967
				17.8	4000	54.6	21.5	-.975
		66.8	15000	8.9	2000	82.3	32.4	-.964
				13.4	3000	65.0	25.6	-.978
				17.8	4000	†	†	†
79	115	51.2	11500	8.9	2000	45.7	18.0	-.972
				13.4	3000	56.6	22.3	-.960
				17.8	4000	55.1	21.7	-.984
		58.7	13200	8.9	2000	†	†	†
				13.4	3000	53.1	20.9	-.968
				17.8	4000	†	†	†
		66.8	15000	8.9	2000	240.8	94.8	-.659
				13.4	3000	112.5	44.3	-.933
				17.8	4000	103.9	40.9	-.940
97	140	51.2	11500	8.9	2000	64.3	25.3	-.825
				13.4	3000	41.9	16.5	-.961
				17.8	4000	46.2	18.2	-.946
		58.7	13200	8.9	2000	75.2	29.6	-.959
				13.4	3000	55.4	21.8	-.975
				17.8	4000	48.3	19.0	-.978
		66.8	15000	8.9	2000	82.6	32.5	-.980
				13.4	3000	83.3	32.8	-.975
				17.8	4000	78.5	30.9	-.967

†Data not available.

TABLE III.- CONCLUDED

(c) Radial-belted tire; $S_{p,max}$ = 35.6 cm (14 in.)

Inflation pressure		F_z		F_x		J_x		r
N/cm^2	lb/in^2	kN	lbs	kN	lbs	cm	in.	
62	90	51.2	11500	8.9 13.4 17.8	2000 3000 4000	∞ ∞ ∞	∞ ∞ ∞	N.A.* N.A.* N.A.*
		58.7	13200	8.9 13.4 17.8	2000 3000 4000	∞ ∞ ∞	∞ ∞ ∞	N.A.* N.A.* N.A.*
		66.8	15000	8.9 13.4 17.8	2000 3000 4000	∞ ∞ ∞	∞ ∞ ∞	N.A.* N.A.* N.A.*
79	115	51.2	11500	8.9 13.4 17.8	2000 3000 4000	∞ ∞ ∞	∞ ∞ ∞	N.A.* N.A.* N.A.*
		58.7	13200	8.9 13.4 17.8	2000 3000 4000	∞ ∞ ∞	∞ ∞ ∞	N.A.* N.A.* N.A.*
		66.8	15000	8.9 13.4 17.8	2000 3000 4000	∞ ∞ ∞	∞ ∞ ∞	N.A.* N.A.* N.A.*
97	140	51.2	11500	8.9 13.4 17.8	2000 3000 4000	∞ ∞ ∞	∞ ∞ ∞	N.A.* N.A.* N.A.*
		58.7	13200	8.9 13.4 17.8	2000 3000 4000	∞ ∞ ∞	∞ ∞ ∞	N.A.* N.A.* N.A.*
		66.8	15000	8.9 13.4 17.8	2000 3000 4000	∞ ∞ ∞	∞ ∞ ∞	N.A.* N.A.* N.A.*

*Not applicable.

III. The data indicate that the decay length values for the bias ply and bias-belted tires may be a function of the loading conditions, but J_x for the radial-belted tire approaches infinite values for all loading conditions.

In order to obtain additional information on the variation of J_x with loading conditions for the bias ply and bias-belted tires a 3^3 factorial ANOVA table (reference 17) was constructed for the bias ply data presented in table III. The results of the tests based on the ANOVA table indicated (with a 90% confidence) that J_x for the bais ply tire was sensitive to variations in the inflation pressure and braking force and insensitive to variations in the vertical load when $S_{p,max}$ was set at 35.6 cm (14 in). This variation of J_x with braking force is contrary to the results presented in reference 14 which reported that the decay length was essentially independent of the braking force.

On the basis of the ANOVA table results, the equations which expressed J_x for the bias ply and bias-belted tires were assumed to be of the form:

$$J_x = \alpha + \eta F_x + \gamma P \tag{9}$$

A multiple regression analysis based on equation (9) produced the following relationships.

$$J_x = 89.03 \text{ cm} - (4.2238 \frac{\text{cm}}{\text{kN}})F_x + (504.8689 \frac{\text{cm}^3}{\text{kN}})P$$

$$J_x = 35.05 \text{ in} - (.0074 \text{ in/lb})F_x + (.1371 \frac{\text{in}^3}{\text{lb}})P$$

with

$$r^2 = .890$$

Bias ply (10)

$$J_x = 128.98 \text{ cm} - (3.3676 \frac{\text{cm}}{\text{kN}})F_x - (122.2585 \frac{\text{cm}^3}{\text{kN}})P$$

$$J_x = 50.78 \text{ in} - (.0059 \text{ in/lb})F_x - (.0332 \frac{\text{in}^3}{\text{lb}})P$$

with

$$r^2 = .800$$

Bias-belted (11)

Equation (10) indicates for the bias ply tire that J_x decreases with the braking force and increases with the inflation pressure. Equation (11) indicates for the bias-belted tire that J_x decreases with either the braking force or the inflation pressure. A comparison of the two equations indicates that the decay lengths for the bias-belted tire are generally higher than those for the bias ply tire for most loading conditions.

Rolling Response

Deformation in the footprint.- The circumferential deformation of the leading half of the rolling footprint during brake application was studied under low speed (≈ 5 knots) conditions. Typical data from these tests are presented in figure 13. Data were obtained under loading conditions which were comparable to those used in the static tests. The deformation at the geometrical center of the footprint, which was observed to be the point of maximum deformation for the bias ply and bias-belted tires, was set equal to F_x/K_x. The deformations of other points within the leading half of the footprint were obtained by substracting the tire deformation accumulated between the center of the footprint and the point in question from F_x/K_x. The values of K_x for each tire were calculated from equations 5, 6, and 7. The data presented in figure 13 indicate that stretching occurs in the footprint of the bias ply and bias-belted tires but not in the footprint of the radial-belted tire during brake application. The tread deformation for the bias ply and bias-belted tires was observed to vary linearly within the rolling footprint.

A numerical measure of this tread deformation was obtained by multiplying the displacements by K_x/F_x to normalize the data and using the least squares method to compute the slope M of the normalized footprint data for each tire under various loading conditions. These data are presented in table IV. The variation of tread deformation with loading conditions was determined for the bias ply and bias-belted tires by assuming an equation for the slope to be of the form

$$M = \alpha + \eta F_x + \beta F_z + \gamma P \qquad (12)$$

A multiple regression analysis of the data presented in table IV yielded the following equations.

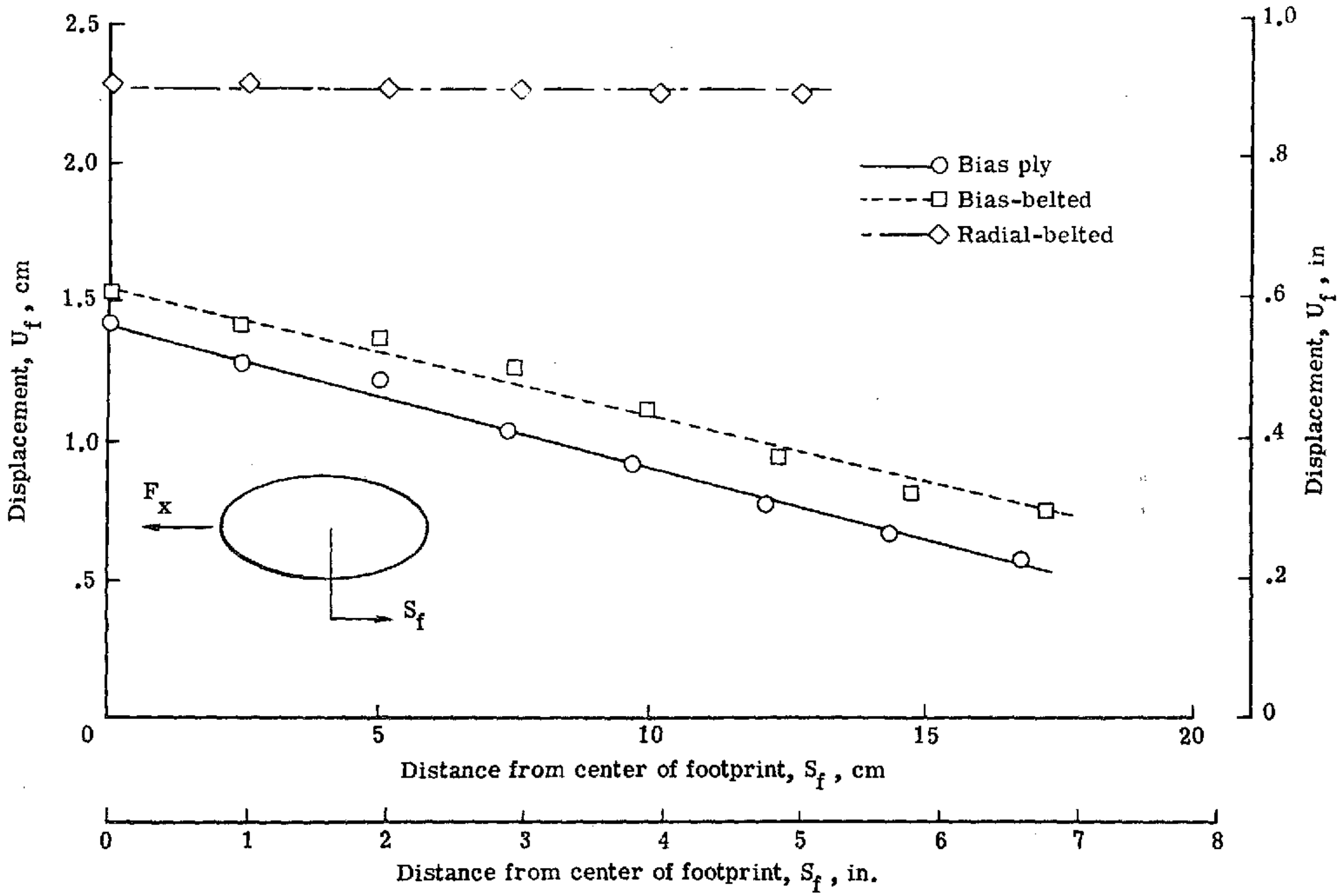

Figure 13.- Typical displacements within footprint of braked-rolling tires.
F_z = 66.8 kN (15,000 lbs); P = 97 N/cm^2 (140 lb/in^2);
$F_x \approx$ 17.8 kN (4000 lbs).

TABLE IV.- SUMMARY OF TREAD DEFORMATION VARIATION WITHIN BRAKED-ROLLING FOOTPRINT

(a) Bias ply tire

P		F_z		h		F_x		M	r
N/cm^2	lb/in^2	kN	lbs	cm	in.	kN	lbs	1/in.	
62	90	51.2	11500	18.80	7.40	9.0	2031	-.060	-.990
						17.6	3960	-.070	-.998
						20.6	4529	-.086	-.994
		58.7	13200	19.51	7.68	10.5	2364	-.038	-.991
						15.9	3567	-.075	-.999
						21.8	4890	-.085	-.998
		66.8	15000	20.29	7.99	10.2	2291	-.049	-.974
						15.6	3500	-.074	-.990
						22.3	5004	-.074	-.999
79	115	51.2	11500	17.53	6.90	9.5	2131	-.050	-.980
						16.6	3725	-.103	-.999
						22.5	5050	-.119	-.995
		58.7	13200	18.97	7.47	9.5	2131	-.054	-.969
						16.8	3783	-.087	-.998
						21.1	4731	-.102	-.999
		66.8	15000	18.82	7.41	10.2	2302	-.055	-.993
						16.5	3698	-.087	-.998
						24.9	4924	-.084	-.999
97	140	51.2	11500	16.13	6.35	8.8	1984	-.076	-.995
		51.2	11500	16.13	6.35	15.2	3422	-.113	-.999
		58.7	13200	17.40	6.85	8.1	1814	-.083	-.986
						15.7	3526	-.109	-.995
						20.6	4638	-.124	-.997
		66.8	15000	17.73	6.98	8.3	1865	-.057	-.984
						17.2	3854	-.094	-.999
						23.1	5181	-.095	-1.000

TABLE IV.- CONTINUED

(b) Bias-belted tire

P		F_z		h		F_x		M	r
N/cm^2	lb/in^2	kN	lbs	cm	in.	kN	lbs	1/in.	
62	90	51.2	11500	19.43	7.65	15.8	3548	-.053	-.992
		51.2	11500	19.43	7.65	19.1	4289	-.065	-.994
		58.7	13200	20.07	7.90	8.6	1931	-.071	-.957
						10.4	2338	-.072	-.986
						13.5	3039	-.071	-.990
		66.8	15000	20.88	8.22	9.2	2065	-.063	-.988
						12.5	2806	-.066	-.995
						19.7	4437	-.065	-.994
79	115	51.2	11500	17.78	7.00	8.9	1992	-.065	-.950
						11.6	2608	-.083	-.991
						17.3	3882	-.101	-.997
		58.7	13200	19.43	7.65	8.9	1998	-.095	-.994
						10.6	2383	-.072	-.982
						12.8	2876	-.082	-.998
		66.8	15000	19.43	7.65	9.5	2137	-.040	-.957
						13.5	3024	-.061	-.997
						18.8	4231	-.073	-.995
97	140	51.2	11500	17.35	6.83	8.0	1803	-.081	-.962
						15.5	3490	-.099	-.991
						18.6	4173	-.088	-.996
		58.7	13200	18.14	7.14	7.2	1611	-.059	-.883
						8.4	1881	-.065	-.982
						10.3	2308	-.072	-.972
		66.8	15000	18.14	7.14	8.9	1992	-.058	-.952
						13.1	2951	-.083	-.995
						18.8	4231	-.080	-.993

TABLE IV.- CONCLUDED

(c) Radial-belted tire

P		F_z		h		F_x		M	r
N/cm^2	lb/in^2	kN	lbs	cm	in.	kN	lbs	1/in.	
62	90	51.2	11500	19.84	7.81	11.0	2468	0	NA*
						14.9	3353	0	NA
						18.5	4151	0	NA
		58.7	13200	19.86	7.82	7.8	1743	0	NA
						11.3	2541	0	NA
						16.9	3803	0	NA
		66.8	15000	20.02	7.88	8.0	1800	0	NA
						11.1	2500	0	NA
						19.1	4300	0	NA
79	115	51.2	11500	18.95	7.46	8.3	1858	0	NA
						14.5	3250	0	NA
						20.7	4649	0	NA
		58.7	13200	18.97	7.47	9.2	2062	0	NA
						11.9	2671	0	NA
						19.8	4442	0	NA
		66.8	15000	19.00	7.48	8.9	2000	0	NA
						11.1	2500	0	NA
						20.0	4500	0	NA
97	140	51.2	11500	18.67	7.35	10.2	2300	0	NA
						15.2	3425	0	NA
						17.8	4000	0	NA
		58.7	13200	18.69	7.36	8.9	2000	†	†
						13.4	3000	†	†
						17.8	4000	†	†
		66.2	15000	18.75	7.38	8.9	2000	†	†
						13.6	3000	†	†
						17.8	4000	†	†

†Data not available.

*Data not applicable.

$$M = -1.03 \times 10^{-2} \frac{1}{cm} - (1.31 \times 10^{-3} \frac{1}{cmkN})F_x + (4.90 \times 10^{-4} \frac{1}{cmkN})F_z - (3.81 \times 10^{-1} \frac{cm}{kN})P$$

$$M = -2.620 \times 10^{-2} \frac{1}{in.} - (1.480 \times 10^{-5} \frac{1}{in.\ lb})F_x + (5.538 \times 10^{-6} \frac{1}{in.\ lb})F_z - (6.669 \times 10^{-4} \frac{in}{lb})P$$

Bias ply

with (13)

$r^2 = .988$

$$M = -3.34 \times 10^{-2} \frac{1}{cm} - (4.20 \times 10^{-4} \frac{1}{cmkN})F_x + (3.39 \times 10^{-4} \frac{1}{cmkN})F_z - (1.26 \times 10^{-1} \frac{cm}{kN})P$$

$$M = -8.447 \times 10^{-2} \frac{1}{in.} - (4.758 \times 10^{-6} \frac{1}{in.\ lb})F_x + (3.839 \times 10^{-6} \frac{1}{in.\ lb})F_z - (2.206 \times 10^{-4} \frac{in}{lb})P$$

Bias-belted

with (14)

$r^2 = .976$

Equations 13 and 14 indicate that the magnitude of M for both tires increases with the braking force and inflation pressure and decreases with the vertical load.

Rolling radius calculations.- The tire deformation data presented in this paper indicate that the elastic response of the aircraft tires to braking forces can be described as a combination of tread stretch and/or torsional wind-up of the tire carcass about the axle. That portion of the tire elastic response which is attributed to tread stretch would be reflected in changes in the tire rolling radius during steady-state brake applications. Therefore, it is appropriate to develop an equation which expresses the change in rolling radius in terms of previously defined tire elastic properties.

The experimental data presented herein indicate that the tread deformation in the leading half of the footprint can be expressed by the following equation

$$u_f = u_{f_0} + m\ S_f \qquad (15)$$

The maximum deformation within the footprint is by definition.

$$u_{f_0} = F_x/K_x \qquad (16)$$

Substitution of equation (16) into (15) and normalizing yields

$$K_x/F_x\ u_f = 1 + MS_f \qquad (17)$$

where

$$M = \frac{m}{u_{f_0}} \qquad (18)$$

The elongation strain in the footprint due to the braking effort is defined to be

$$\varepsilon_{x,f} = \frac{du_f}{dS_f} = \frac{F_x}{K_x} M \tag{19}$$

The tread stretch which has accumulated within the footprint can be determined by integrating equation (19) over the half length of the footprint to yield

$$Q_f = \int du_f = \frac{F_x}{K_x} M \int_h^0 dS_f = \frac{F_x}{K_x} MS_f\Big]_h^0 = -\frac{F_x}{K_x} Mh \tag{20}$$

The static data presented herein indicated that the tread deformation along the free-tread periphery near the footprint leading edge can be expressed as

$$u_p = \frac{F_x}{K_x} e^{-\frac{S_p}{J_x}} \tag{21}$$

$$\text{for} \quad 0 \leq S_p \leq S_{p,max}$$

and the maximum deformation was assumed to occur at the footprint leading edge. Under rolling conditions, however, equation (21) must be modified to conform to the following boundary condition.

$$\left[u_f \Big|_{S_f = h} = u_p \Big|_{S_p = 0} \right] \tag{22}$$

where

$$u_f \Big|_{S_f = h} = \frac{F_x}{K_x} + mh \tag{23}$$

Equation (21) now becomes

$$u_p = \frac{F_x}{K_x} (1 + Mh) e^{-\frac{S_p}{J_x}} \tag{25}$$

$$0 \leq S_p \leq S_{p,max}$$

The elongation strain in the free-tread periphery due to the braking effort is defined by

$$\varepsilon_{x,p} = \frac{du_p}{dS_p} = - \frac{F_x}{J_x K_x} (1 + Mh) e^{-\frac{S_p}{J_x}} \tag{26}$$

The tread stretch which has accumulated in the free-tread periphery can be determined by integrating equation (26) over the appropriate limits of integration

$$Q_p = \int du_p = \frac{F_x}{K_x} (1 + Mh) \int_{S_{p,max}}^{0} - \frac{1}{J_x} e^{-\frac{S_p}{J_x}} dS_p \tag{27}$$

Performing the indicated integration yields

$$Q_p = \frac{F_x}{K_x} (1 + Mh) e^{-\frac{S_p}{J_x}} \Big]_{S_{p,max}}^{0} \tag{28}$$

or

$$Q_p = \frac{F_x}{K_x} (1 + Mh)(1 - e^{-\frac{S_{p,max}}{J_x}}) \tag{29}$$

The total tread stretch due to the braking effort is the sum

$$Q_T = Q_f + Q_p \tag{30}$$

Equation (30) then represents the net increase in tire circumference due to braking forces and the net change in rolling radius is obtained by dividing equation (30) through by 2π to yield

$$\Delta R = \frac{Q_T}{2\pi} = \frac{F_x}{2\pi K_x}\left[-Mh + (1 + Mh)(1 - e^{-\frac{S_{p,max}}{J_x}})\right] \tag{31}$$

Equation 31 is a general expression which may be used to compute the change in rolling radius due to the braking effort regardless of the tire construction. It should be noted, however, that equation 31 is considerably different from the expressions for computing ΔR which were developed in references 13 and 14 wherein ΔR was equated to the product of the tire unloaded radius and the maximum value of the circumferential strain of the tread. Furthermore, on the basis of the analysis presented in this paper it would appear that the expressions for computing ΔR presented in references 13 and 14 are in error and would overestimate the net change in the tire rolling radius by a factor of 2π.

Application of Results

Apparent change in rolling radius.- Experimental braked-and unbraked rolling tests were conducted to determine the apparent change in rolling radius (or wheel slippage) of the bias ply, bias-belted, and radial-belted tires under various loading conditions. In each case the apparent rolling radius was determined by relating the distance traveled to the number of wheel revolutions.

$$R_b \text{ or } R_0 = \frac{D}{2\pi N} \tag{33}$$

The experimental change in rolling radius is the difference between the apparent rolling radii of the braked and the freely rolling tire.

$$\Delta R_{exp} = R_b - R_0 \tag{33}$$

When computed in this manner ΔR_{exp} includes both the effective change in rolling radius due to tire slippage within the tire-pavement interface and the actual change in rolling radius due to the elastic deformation of the tire tread.

Values of ΔR_{exp} for each tire are presented in table V. The calculated values of change in rolling radius ΔR_{cal}, also presented in table V, are based upon equation 31. For the purpose of these calculations the values of K_x, J_x, and M for the bias ply and bias-belted tires were computed from equations 5 and 6, 10 and 11, and 13 and 14 respectively. The values of K_x for the radial-belted tire

TABLE V.- SUMMARY OF ROLLING RADIUS DATA

(a) Bias ply tire

Speed knots	P		F_z		F_x		ΔR_{cal}*		ΔR_{exp}	
	N/cm^2	lb/in^2	kN	lbs	kN	lbs	cm	in	cm	in
5	97	140	56.3	12664	19.2	4324	.19	.07	2.34	.92
5	97	140	62.3	14007	18.5	4165	.18	.07	1.68	.66
5	79	115	56.8	12761	20.2	4531	.21	.08	2.39	.94
5	79	115	64.5	14486	19.0	4268	.18	.07	2.16	.85
5	62	90	55.5	12477	16.9	3788	.16	.06	1.96	.77
5	62	90	64.5	14492	15.7	3526	.12	.05	1.42	.56
5	97	140	70.9	15926	14.5	3254	.10	.04	1.73	.68
5	79	115	72.6	16311	15.7	3528	.11	.04	1.73	.68
5	62	90	70.9	15926	15.7	3528	.10	.04	1.73	.68
98.0	97	140	58.6	13161	8.7	1957	.06	.02	.71	.28
98.0	97	140	57.6	12950	15.2	3425	.12	.05	1.50	.59
97.3	97	140	57.9	13022	20.5	4606	.22	.09	2.13	.84
100.0	97	140	66.9	15035	19.3	4326	.18	.07	1.88	.74
103.0	97	140	65.7	14773	14.4	3238	.11	.04	1.37	.54
104.0	97	140	65.5	14768	9.4	2110	.06	.02	.74	.29
103.0	97	140	72.7	16333	8.8	1985	.04	.02	.66	.26
99.0	97	140	72.6	16308	15.1	3400	.11	.04	1.32	.52
98.0	97	140	73.6	16543	20.6	4624	.18	.07	1.91	.75
99.0	79	115	58.7	13196	13.5	3023	.11	.04	2.08	.82
99.0	79	115	58.4	13119	14.1	3167	.12	.05	1.47	.58
103.0	79	115	57.8	12998	8.3	1873	.05	.02	.71	.28
100.0	79	115	57.3	12879	8.8	1973	.05	.02	.74	.29
104.0	79	115	65.5	14710	15.8	3545	.12	.05	1.35	.53
101.0	79	115	69.3	15583	20.9	4689	.20	.08	1.96	.77
101.0	79	115	74.0	16618	19.4	4367	.16	.06	1.65	.65
102.0	79	115	73.0	16404	15.1	3404	.10	.04	1.22	.48
103.0	79	115	71.4	16046	10.2	2295	.05	.02	.64	.25
107.0	62	90	56.8	12757	8.9	2010	.05	.02	.51	.20
107.0	62	90	56.8	12753	15.6	3515	.13	.05	1.55	.61
107.0	62	90	57.2	12851	17.1	3841	.16	.06	1.98	.78
99.0	62	90	66.0	14821	18.6	4172	.16	.06	1.63	.64
99.5	62	90	64.3	14439	15.0	3370	.11	.04	1.32	.52
97.0	62	90	66.3	14893	20.7	4658	.20	.08	1.73	.68
100.0	62	90	72.2	16225	20.4	4579	.18	.07	1.42	.56
101.0	62	90	71.9	16156	14.7	3304	.09	.03	.91	.36
100.0	62	90	72.9	16376	9.4	2118	.03	.01	.46	.18

*From equation 31.

TABLE V.- CONTINUED

(b) Bias-belted tire

Speed, knots	P		F_z		F_x		ΔR_{cal}*		ΔR_{exp}	
	N/cm^2	lb/in^2	kN	lbs	kN	lbs	cm	in	cm	in
5	97	140	70.1	15472	13.7	3084	.08	.03	1.17	.46
5	79	115	70.9	15936	14.4	3229	.10	.04	†	†
5	62	90	69.6	15648	16.5	3710	.14	.05	1.45	.57
5	97	140	56.0	12578	6.9	1556	.04	.02	.41	.16
5	97	140	64.1	14404	14.6	3288	.10	.04	1.47	.58
5	79	115	55.6	12484	15.0	3374	.11	.04	1.55	.61
5	79	115	63.2	14213	15.3	3433	.12	.05	1.40	.55
5	62	90	54.7	12293	15.5	3491	.14	.05	1.30	.51
98.7	97	140	58.8	13204	14.6	3289	.10	.04	.94	.37
100.4	97	140	61.3	13767	11.3	2543	.07	.03	.79	.31
101.6	97	140	65.6	14732	11.1	2500	.07	.03	.79	.31
102.3	97	140	63.3	14231	8.5	1914	.05	.02	.91	.36
97.5	97	140	51.1	12826	8.5	1902	.05	.02	.56	.22
98.7	79	115	66.5	14952	8.3	1857	.05	.02	.89	.35
98.7	62	90	58.3	13101	11.3	2543	.09	.04	.86	.34
100.6	79	115	72.3	16249	9.6	2167	.06	.02	.46	.18
98.8	79	115	72.9	16379	12.0	2699	.08	.03	.33	.13
99.7	79	115	73.1	16430	16.3	3660	.11	.04	1.02	.40
97.2	79	115	67.0	15064	11.7	2638	.08	.03	.74	.29
98.5	79	115	67.4	15154	16.1	3626	.12	.05	.86	.34
103.0	97	140	73.9	16615	8.6	1924	.04	.02	.41	.16
98.9	97	140	71.4	16049	12.3	2773	.07	.03	.74	.29
100.2	97	140	73.6	16550	14.7	3305	.09	.03	.94	.37
94.3	97	140	68.1	15311	15.2	3424	.10	.04	1.63	.64
97.2	79	115	58.5	13145	8.5	1918	.06	.02	.48	.19
97.2	79	115	59.8	13430	11.2	2509	.08	.03	.71	.28
97.2	79	115	60.6	13623	14.7	3295	.11	.04	.94	.37
101.0	62	90	59.2	13297	14.0	3149	.11	.04	.79	.31
101.0	62	90	67.0	15064	8.5	1915	.06	.02	.41	.16
97.5	62	90	65.5	14719	11.3	2535	.09	.03	.69	.27
97.5	62	90	67.2	15109	14.5	3248	.12	.05	1.02	.40
98.8	62	90	74.7	16789	8.8	1974	.06	.02	.38	.15
96.0	62	90	73.0	16404	11.9	2669	.09	.03	.53	.21
99.7	62	90	74.3	16692	15.4	3459	.12	.05	.91	.36
100.6	79	115	67.5	15158	16.8	3773	.12	.05	1.12	.44
89.0	79	115	58.9	13239	19.8	4455	.16	.06	1.02	.40
101.0	79	115	59.3	13333	18.8	4216	.15	.06	1.80	.71
93.5	79	115	58.9	13239	18.8	4216	.15	.06	1.40	.55
98.7	62	90	58.3	13105	8.9	2009	.07	.03	.28	.11

*From equation 31.

†Data not available.

TABLE V.- CONCLUDED

(c) Radial-belted tire.

Speed, knots	P		F_z		F_x		ΔR_{cal}*		ΔR_{exp}	
	N/cm^2	lb/in^2	kN	lbs	kN	lbs	cm	in	cm	in
5	97	140	51.2	11500	9.6	2150	0	0	.48	.19
5	97	140	58.7	13200	11.3	2550	0	0	.46	.18
5	97	140	66.8	15000	13.5	3025	0	0	.25	.10
5	79	115	51.2	11500	11.1	2500	0	0	.35	.14
5	79	115	58.7	13200	11.8	2650	0	0	.19	.08
5	79	115	66.8	15000	14.0	3150	0	0	.24	.10
5	62	90	51.2	11500	12.0	2700	0	0	.26	.10
5	62	90	58.7	13200	14.7	3300	0	0	.21	.08
5	62	90	66.8	15000	16.1	3625	0	0	.21	.08
97.1	97	140	66.5	14952	8.5	1902	0	0	.21	.08
101.0	97	140	58.1	13047	5.7	1277	0	0	.13	.05
100.2	97	140	59.2	13293	11.8	2646	0	0	.36	.14
101.1	79	115	66.4	14924	7.4	1663	0	0	.10	.04
101.5	79	115	67.0	15061	10.7	2404	0	0	.13	.05
100.6	79	115	65.1	14620	13.4	3022	0	0	.15	.06
99.2	97	140	66.2	14867	7.1	1586	0	0	.21	.08
98.3	97	140	66.6	14964	10.9	2448	0	0	.33	.13
97.7	97	140	67.4	15139	14.5	3248	0	0	.41	.16
101.1	79	115	58.9	13239	8.0	1802	0	0	.13	.05

*From equation 31.

were computed from equation 7 and the values of J_x and M were set equal to ∞ and 0 respectively. The footprint half-lengths were obtained from table IV and the value of $S_{p,max}$ was set equal to 35.6 cm (14 in) for all test conditions. The changes in rolling radius during braking as calculated from equation 31 are compared in figure 14 with those obtained experimentally. The tire slip boundary is defined by the straight line near the left edge of the figure. The data indicate that a major portion of the apparent change in rolling radius of the bias ply and bias-belted tires and virtually all the apparent change in rolling radius of the radial-belted tire measured experimentally is due to an actual tire slippage within the tire-pavement interface.

Tire slip.- Once the actual change in rolling radius due to tire elastic deformation has been established, the amount of tire slippage which occurs in the tire-pavement interface during braking can be determined from the following equation

$$X_T = 2\pi(\Delta R_{exp} - \Delta R_{cal}) \tag{34}$$

where X_T is the tire skidding distance per wheel revolution. The braking force friction coefficient μ_x is a measure of the braking effort and is defined as

$$\mu_x = \frac{F_x}{F_z} \tag{35}$$

The variation of the μ_x with tire slip for the bias ply, bias-belted,

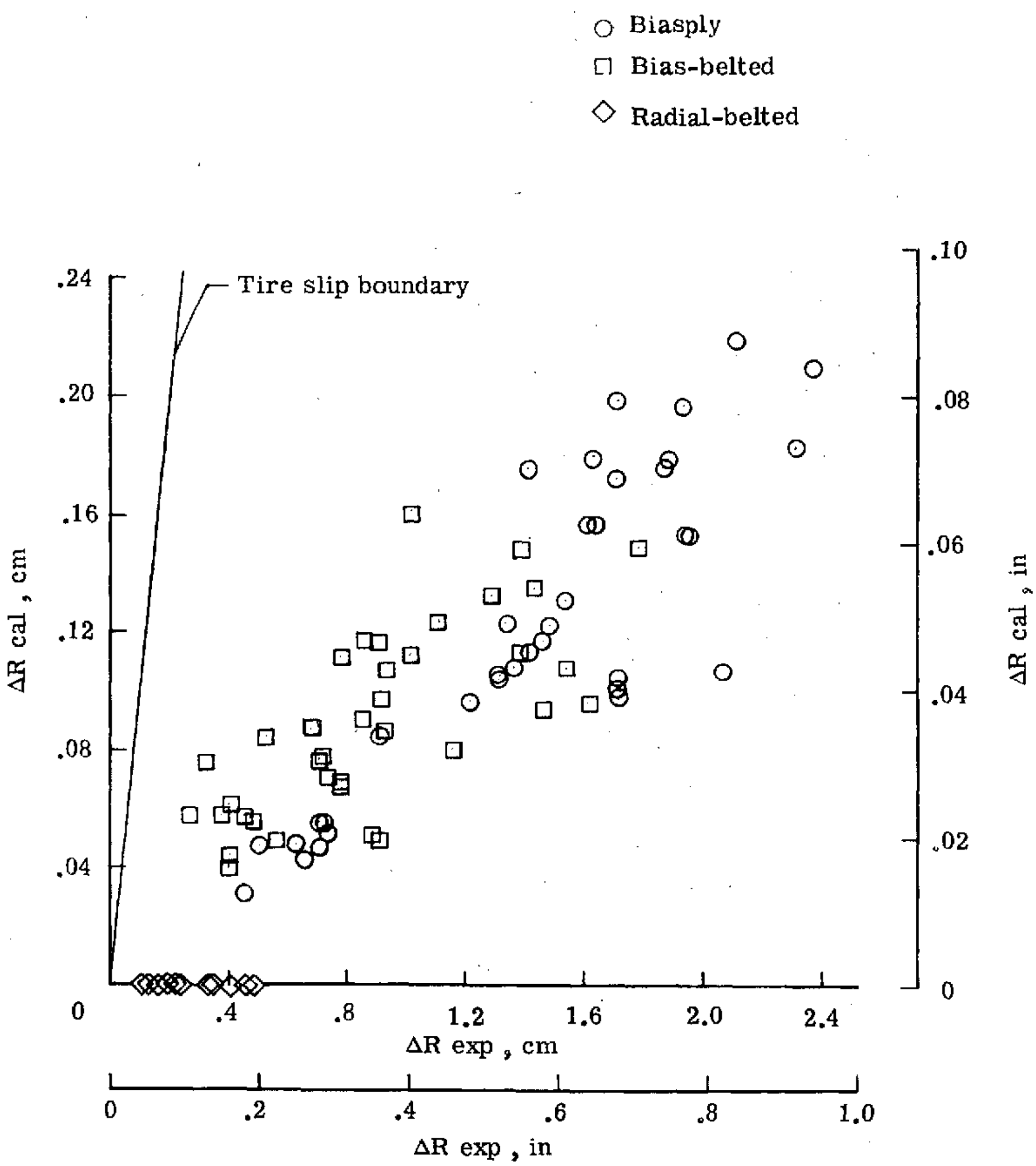

Figure 14.- Comparison of calculated and experimental change in rolling radius attributed to braking.

and radial-belted tires are presented in figure 15. The values of μ_x and X_T plotted in the figure were computed from the data presented in table V. The equations for the faired curves in the figure were determined by the least squares method and are listed below.

$$\left.\begin{aligned} \mu_x &= .037 + (.024 \tfrac{1}{cm})X_T \\ \mu_x &= .037 + (.061 \tfrac{1}{in})X_T \\ &\text{with} \\ r &= .88 \end{aligned}\right\} \text{Bias ply} \qquad (36)$$

$$\left.\begin{aligned} \mu_x &= .030 + (.034 \tfrac{1}{cm})X_T \\ \mu_x &= .030 + (.086 \tfrac{1}{in})X_T \\ &\text{with} \\ r &= .74 \end{aligned}\right\} \text{Bias-belted} \qquad (37)$$

$$\left.\begin{aligned} \mu_x &= -.069 + (.158 \tfrac{1}{cm})X_T \\ \mu_x &= -.069 + (.402 \tfrac{1}{in})X_T \\ &\text{with} \\ r &= .41 \end{aligned}\right\} \text{Radial-belted} \qquad (38)$$

The small value of r for the radial-belted data is caused by the nearly vertical slope of the faired curve (figure 15) rather than by a

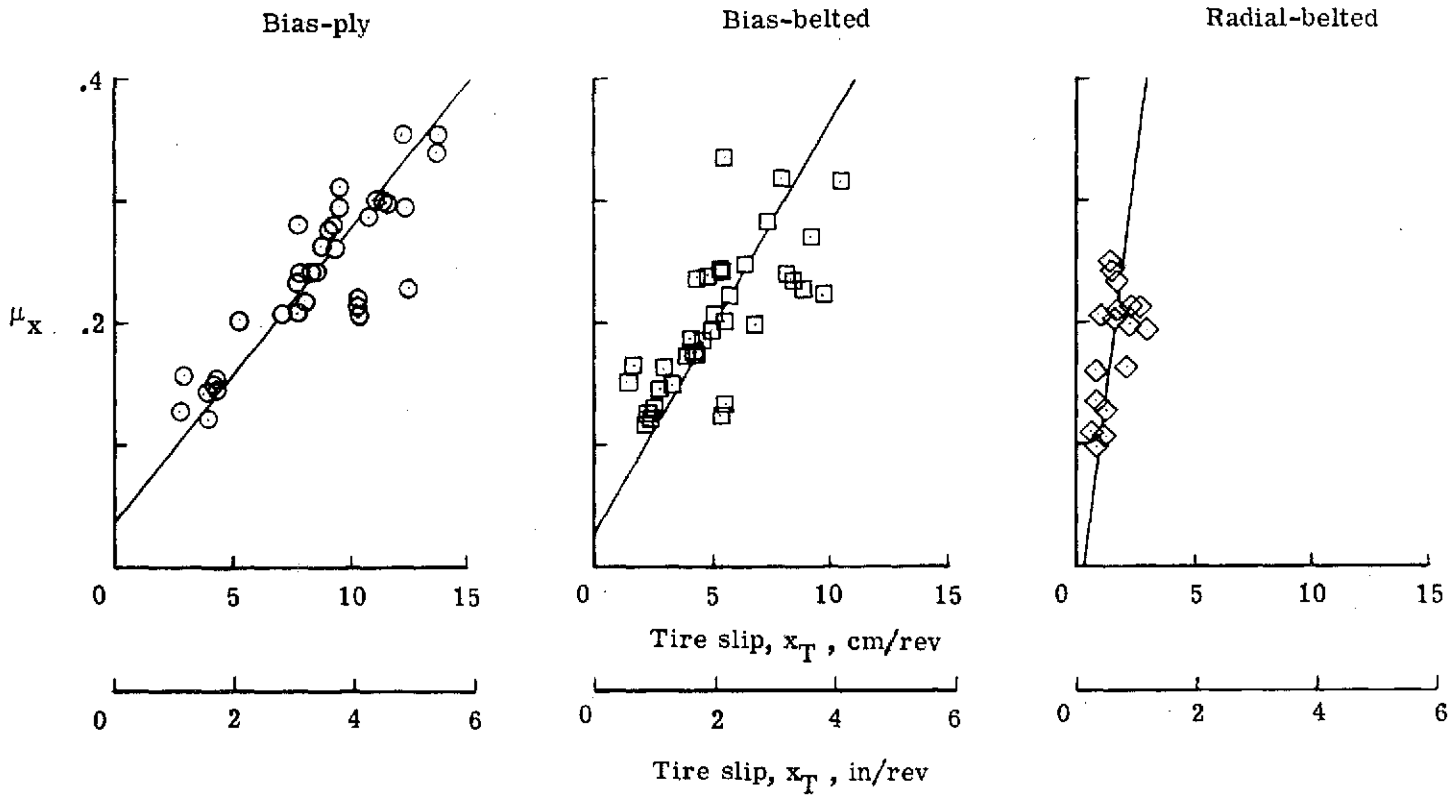

Figure 15.- Braking friction coefficient vs. tire slip.

lack of data correlation. These data indicate that the bias ply tire is subjected to the most severe tire slippage and the radial-belted tire is subjected to the least severe tire slippage during braking operations.

Final remarks.- The results of this investigation have several implications which are of interest to aircraft landing gear and antiskid braking system designers. The tire slippages noted for the three tire designs imply higher wear rates for the bias ply tire than for the bias-belted or radial-belted tires during braking and other ground maneuver operations. The reduced tire slippages noted for the belted tire designs could also result in lower tread temperatures which suggest improved traction performance for braking and steering. The fore-and-aft spring constant values observed for each tire design indicate that a stifferspring coupling between the brake and the tire-pavement interface would be associated with the bias-belted and bias ply tires than with the radial-belted tire. Unless properly handled, these variations in spring couplings may seriously degrade the performance of aircraft antiskid braking systems and reduce or possibly eliminate any advantages gained by using belted tire designs. Therefore, when deciding on a tire design for aircraft applications the landing gear and antiskid braking system designers must weigh the possible advantages of belted designs against the possible degradation, in antiskid braking system performance resulting from the variation in the tire fore-and-aft elastic response characteristics.

CONCLUSIONS

Tests were conducted to determine the fore-and-aft elastic response characteristics of size 34.99, type VII aircraft tires of bias ply, bias-belted, and radial-belted design. These characteristics which include the static fore-and-aft spring constant, fore-and-aft decay length along the free-tread periphery, and deformations variation within the rolling footprint were obtained over a range of vertical loads from 51.2 kN (11,500 lbs) to 66.8 kN (15,000 lbs) and inflation pressures from 62 N/cm^2 (90 lb/in^2) to 97 N/cm^2 (140 lb/in^2) at ground speeds up to 100 knots and at braking forces up to 22.3 kN (5000 lbs). The investigation consisted of static and rolling tests at the Langley Aircraft Landing Loads and Traction Facility, a statistical analysis which related the measured tire elastic characteristics to variations in the vertical load, inflation pressure, braking force, and/or tire vertical deflection, and a semi-empirical analysis which related tire elastic behavior to measured wheel slippage during steady-state braking. The results of these tests suggest the following conclusions.

The bias-belted tire was shown to have the largest spring constant value for most loading conditions and the radial-belted tire was shown to have the smallest spring constant value for all loading conditions. The static fore-and-aft spring constant was shown (1) to decrease with tire vertical deflection and to increase with inflation pressure for each of the three tires and (2) to increase with vertical load for the bias ply tire and to decrease with vertical load for the bias-belted and radial-belted tires.

The elastic response of the tire free-tread periphery to static braking was shown to include both tread stretch and carcass torsional wind-up about the axle for the bias ply and bias-belted tires and carcass wind-up alone for the radial-belted tire. The bias-belted tire was shown to have larger decay length values than the bias ply tire for most loading conditions while the decay lengths for the radial-belted tire approached infinite values thereby denoting the lack of tread stretch during brake application. The fore-and-aft decay length was shown (1) to be insensitive to variations in the vertical load and to decrease with braking force for both the bias ply and bias-belted tires and (2) to increase with inflation pressure for the bias ply tire and to decrease with inflation pressure for the bias-belted tire.

Tread stretching under braked rolling conditions was detected within the footprints of the bias ply and bias-belted tires but not within the footprint of the radial-belted tire. The magnitude of tread deformation variations within the footprints of the bias ply and bias-belted tires was shown to increase with braking force and inflation pressure and to decrease with vertical load.

It was demonstrated that changes in rolling radius due to braking can be predicted with reasonable accuracy from the elastic fore-and-aft response characteristics of the tires. These changes in rolling radius can then be used in conjunction with the experimentally determined wheel response characteristics to calculate the actual tire slippage under steady-state braked rolling conditions. Tire slippage during steady-state braking was shown to be greater for the bias ply than for the bias-belted and radial-belted tires. Finally, when deciding on tire designs for aircraft applications, the landing gear and brake system designers must weigh the possible advantages of belted designs such as improved tread life and tire traction performance against the possible degradation in antiskid braking system performance resulting from the variation in the tire fore-and-aft elastic response characteristics.

REFERENCES

1. Davis, J. E. and Curry, R. C.: The Costs of Landing an Airplane. SAE Journal, Vol. 71, No. 12, December 1963, pp. 47-50.

2. Batterson, Sidney, A.: A Study of the Dynamics of Airplane Braking Systems as Affected by Tire Elasticity and Brake Response. NASA TN D-3081, 1965.

3. Tanner, John A.: Performance of an Aircraft Tire Under Cyclic Braking Conditions and of a Currently Operational Antiskid Braking System. NASA TN D-6755, 1972.

4. Carbon, Christian Bourcer de: Étude Théorique du Shimmy des Roues d'Avion (Analytical Study of Shimmy of Airplane Wheels). Office National d'Etude et de Recherches Aéronautiques, Publication No. 7, 1948 (Available in English Translation as NACA TM 1337.)

5. Förster, B.: Versuche zur Feststellung des Haftvermögens von Personenwagen - Bereifungen. Deutsche Kraftfahrtforschung zb. No. 22 (Berlin), (Undated). (Available in English Translation as NACA TM 1416.)

6. Fromm, H.: Seitenschluph und Führungswert des rollenden Rades (Sideslip and Guiding Characteristics of the Rolling Wheel.) Bericht 140 der L.GL., 1941, pp. 56-63 (Available in English Translation as NACA TM 1365, pp. 191-216.)

7. Fromm, H.: Schwingungsdämpfung am rollender Rade. (Oscillation Damping on the Rolling Wheel) Bericht 140 der L.GL., 1941, pp. 66-67. (Available in English Translation as NACA TM 1365, pp. 229-233.)

8. Horne, Walter B.: Static Force-Deflection Characteristics of Six Aircraft Tires Under Combined Loading. NACA TN 2926, 1953.

9. Horne, Walter B.; Stephenson, Bertrand H.; and Smiley, Robert F.: Low-Speed Yawed-Rolling Characteristics of Two 56-Inch-Diameter, 24 Ply-Rated, Type VII Aircraft Tires. NACA TN 3235, 1954.

10. Horne, Walter B. and Smiley, Robert F.: Low-Speed Yawed-Rolling Characteristics and other Elastic Properties of a Pair of 40-Inch-Diameter, 14 Ply-Rated, Type VII Aircraft Tires. NACA TN 4109, 1958.

11. Kantrowitz, Arthur: Stability of Castering Wheels for Aircraft Landing Gears. NACA Rep. 686, 1940.

12. Boeckh: Ermittlung der elastischen konstanten von Flugzeugreifen (Determination of the Elastic Constants of Airplane Tires). Focke-Wulf Flugzeughau G.m.b.H. (Bermen), Dec. 1944. (Available in English Translation as NACA TM 1378.)

13. Smiley, Robert F. and Horne, Walter B.: Mechanical Properties of Pneumatic Tires With Special Reference to Modern Aircraft Tires. NASA TR R-64, 1960. (Supersedes NACA TN 4110.)

14. Tanner, John A.; McCarty, John L.; and Batterson, Sidney A.: The Elastic Response of Bias-Ply Aircraft Tires to Braking Forces. NASA TN D-6426, 1971.

15. Hoel, Paul G.: Introduction to Mathematical Statistics. Third Edition, John Wiley and Sons, Inc. New York, N.Y., 1962.

16. Draper, N. R. and Smith, H.: Applied Regression Analysis. John Wiley and Sons, Inc., New York, N. Y. 1966.

17. Hicks, Charles R.: Fundamental Concepts in the Design of Experiments. Holt, Rinehart, and Winston, Chicago, Ill., 1964.